

# An Experimental and Quantum Chemical Investigation of CO Binding to Heme Proteins and Model Systems: A Unified Model Based on $^{13}\text{C}$ , $^{17}\text{O}$ , and $^{57}\text{Fe}$ Nuclear Magnetic Resonance and $^{57}\text{Fe}$ Mössbauer and Infrared Spectroscopies

Michael T. McMahon,<sup>†</sup> Angel C. deDios,<sup>‡</sup> Nathalie Godbout, Renzo Salzmann, David D. Laws,<sup>§</sup> Hongbiao Le,<sup>||</sup> Robert H. Havlin,<sup>§</sup> and Eric Oldfield\*

Contribution from the Department of Chemistry, University of Illinois at Urbana–Champaign, 600 South Mathews Avenue, Urbana, Illinois 61801

Received September 17, 1997

**Abstract:** We have investigated the question of how CO ligands bind to iron in metalloporphyrins and metalloproteins by using a combination of nuclear magnetic resonance (NMR),  $^{57}\text{Fe}$  Mössbauer, and infrared spectroscopic techniques, combined with density functional theoretical calculations to analyze the spectroscopic results. The results of  $^{13}\text{C}$  NMR isotropic chemical shift,  $^{13}\text{C}$  NMR chemical shift anisotropy,  $^{17}\text{O}$  NMR isotropic chemical shift,  $^{17}\text{O}$  nuclear quadrupole coupling constant,  $^{57}\text{Fe}$  NMR isotropic chemical shift,  $^{57}\text{Fe}$  Mössbauer quadrupolar splitting, and infrared measurements indicate that CO binds to Fe in a close to linear fashion in all conformational substates. The  $^{13}\text{C}$ -isotropic shift and shift anisotropy for an  $\text{A}_0$  substate model compound: Fe(5,10,15,20-tetraphenylporphyrin)(CO)(*N*-methylimidazole), as well as the  $^{17}\text{O}$  chemical shift, and the  $^{17}\text{O}$  nuclear quadrupole coupling constant (NQCC) are virtually the same as those found in the  $\text{A}_0$  substate of *Physeter catodon* CO myoglobin and lead to most probable ligand tilt ( $\tau$ ) and bend ( $\beta$ ) angles of  $0^\circ$  and  $1^\circ$  when using a Bayesian probability or *Z* surface method for structure determination. The infrared  $\nu_{\text{CO}}$  for the model compound of  $1969\text{ cm}^{-1}$  is also that found for  $\text{A}_0$  proteins. Results for the  $\text{A}_1$  substate (including the  $^{57}\text{Fe}$  NMR chemical shift and Mössbauer quadrupole splitting) are also consistent with close to linear and untilted Fe–C–O geometries ( $\tau = 4^\circ$ ,  $\beta = 7^\circ$ ), with the small changes in ligand spectroscopic parameters being attributed to electrostatic field effects. When taken together, the  $^{13}\text{C}$  shift,  $^{13}\text{C}$  shift anisotropy,  $^{17}\text{O}$  shift,  $^{17}\text{O}$  NQCC,  $^{57}\text{Fe}$  shift,  $^{57}\text{Fe}$  Mössbauer quadrupole splitting, and  $\nu_{\text{CO}}$  all strongly indicate very close to linear and untilted Fe–C–O geometries for all carbonmonoxyheme proteins. These results represent the first detailed quantum chemical analysis of metal–ligand geometries in metalloproteins using up to seven different spectroscopic observables from three types of spectroscopy and suggest a generalized approach to structure determination.

## Introduction

How small ligands such as CO, O<sub>2</sub>, RNC, RNO, NO, and N<sub>3</sub><sup>−</sup> bind to metalloproteins and metalloporphyrins has been a topic of interest for some time,<sup>1–4</sup> because of the obvious importance of especially O<sub>2</sub> carriers in respiration, and more recently of NO and CO ligands as regulators of cell and organ

function.<sup>5</sup> Typically, X-ray crystallographic methods have been used to deduce metal–ligand geometries, but quite large variabilities appear to exist between different structures. For example, Fe–C–O bond angles from  $176^\circ$  to  $118^\circ$  have been reported,<sup>6,7</sup> Fe–O–O angles from  $159^\circ$  to  $115^\circ$  have been described,<sup>8,9</sup> Fe–C–N angles of  $180^\circ$  to  $96^\circ$  have been observed in alkyl isocyanide adducts,<sup>10,11</sup> etc., and it is unclear to what extent these differences are real. In the case of CO, the results of infrared and Raman spectroscopy have been used to deduce a close-to-linear and untilted Fe–C–O geometry,<sup>12,13</sup> with the changes in the observables being attributed to electrostatic field

<sup>†</sup> National Institutes of Health Molecular Biophysics Training Grant Trainee (grant GM-08276).

<sup>‡</sup> Present address: Department of Chemistry, Georgetown University, 37th and O Streets, N.W., Washington, DC 20057-2222.

<sup>§</sup> Present address: Department of Chemistry, University of California, Berkeley, CA 94720.

<sup>||</sup> Present address: Laboratorium für Physicalische Chemie, ETH, Universitätstr. 22, 8092, Zürich, Switzerland.

(1) Pauling, L.; Coryell, C. D. *Proc. Natl. Acad. Sci. U.S.A.* **1936**, *22*, 210–216.

(2) Pauling, L. *Nature* **1964**, *203*, 182–183. Weiss, J. J. *Nature* **1964**, *203*, 182–183.

(3) St. George, R. C.; Pauling, L. *Science* **1951**, *114*, 629–634. Lein, A.; Pauling, L. *Proc. Natl. Acad. Sci. U.S.A.* **1956**, *42*, 51–54.

(4) Filehne, W. *Arch. Exptl. Pathol. Pharmacol.* **1878**, *9*, 329–379. Wärburg, O.; Kubowitz, T.; Christian, W. *Biochem. Z.* **1931**, *242*, 170–205. Jung, F. *Naturwissenschaften* **1940**, *28*, 264–265. Keilin, D.; Hartree, E. F. *Nature* **1943**, *151*, 390–391.

(5) Suematsu, M.; Wakabayashi, Y.; Ishimura, Y. *Cardiovas. Res.* **1996**, *32*, 679–686.

(6) Quillin, M. L.; Arduini, R. M.; Olson, J. S.; Phillips, G. N., Jr. *J. Mol. Biol.* **1993**, *234*, 140–155.

(7) Kuriyan, J.; Wilz, S.; Karplus, M.; Petsko, G. A. *J. Mol. Biol.* **1986**, *192*, 133–154.

(8) Shaanan, B. *J. Mol. Biol.* **1983**, *171*, 31–59. Steigemann, W.; Weber, E. In *Hemoglobin and Oxygen Binding*; Ho, C., Ed.; Elsevier Biomedical: New York, 1982; pp 19–24.

(9) Phillips, S. E. V. *J. Mol. Biol.* **1980**, *142*, 531–554.

(10) Mims, M. P.; Olson, J. S.; Russu, I. M.; Miura, S.; Cedel, T. E.; Ho, C. *J. Biol. Chem.* **1983**, *258*, 6125–6134.

effects, much as with our own NMR/IR correlations.<sup>14–16</sup> However, very recent crystallographic results on carbonmonoxymyoglobin again suggest distorted ( $\sim 45\text{--}55^\circ$ ) Fe–C–O bonding,<sup>17</sup> consistent with earlier crystallographic results<sup>7,18</sup> and with XANES and EXAFS results.<sup>19,20</sup> Distortions have also been suggested from solid-state NMR<sup>21</sup> and from some Mössbauer work.<sup>22,23</sup> Given the fact that IR/Raman experiments are more difficult with non-CO ligands, and that the actual detailed assignments themselves are not always simple to make,<sup>24</sup> it therefore seems to be desirable to explore the possibilities of using a variety of spectroscopic observables to investigate metal–ligand bonding. In this paper, we use up to six additional spectroscopic parameters, the isotropic carbon-13 NMR chemical shift ( $\delta_i$ ,  $^{13}\text{C}$ ), the  $^{13}\text{C}$  NMR chemical shift anisotropy (CSA) ( $\Delta\delta$ ,  $^{13}\text{C}$ ), the isotropic oxygen-17 NMR chemical shift ( $\delta_i$ ,  $^{17}\text{O}$ ), the  $^{17}\text{O}$  nuclear quadrupole coupling constant (NQCC) ( $e^2qQ/h$ ,  $^{17}\text{O}$ ), the isotropic iron-57 NMR chemical shift ( $\delta_i$ ,  $^{57}\text{Fe}$ ), the iron-57 Mössbauer quadrupole splitting ( $\Delta E_Q$ ,  $^{57}\text{Fe}$ ), and the CO infrared stretch frequency ( $\nu_{\text{CO}}$ ), to test various structural models, using parameter surfaces and the Bayesian probability method reported previously for amino acids.<sup>25,26</sup> The methods described are general and show how NMR, Mössbauer, and IR techniques can all be used together to develop and test models of metal–ligand interactions in metalloproteins, by using quantum chemical methods to make the necessary correlations between the spectroscopic observables and structure.

## Experimental Section

**Chemical Aspects.** The synthesis and characterization of the model compound Fe(5,10,15,20-tetraphenylporphyrin)(CO)(*N*-methylimidazole) will be described in detail elsewhere<sup>27</sup> and basically followed standard methods.<sup>28</sup> The exception is that two samples were prepared. The first was prepared in a “standard” fashion in that solvent was removed from crystals in vacuo, while in a second sample the mother liquor was retained, in an effort to retain good quality crystals for solid-state NMR. CO ( $^{13}\text{CO}$ , 99%; Cambridge Isotope Laboratories, Andover, MA;  $\text{C}^{17}\text{O}$ , 37%, Icon Services, Inc., Summit, NJ) gas exchange was achieved prior to crystallization using a Pd/ $\text{Al}_2\text{O}_3$  heterogeneous catalyst.<sup>29</sup> Here, approximately 100 mg Fe(TPP)(CO)(NMeIm) (TPP = 5,10,15,20-tetraphenylporphyrin; NMeIm = *N*-methylimidazole) was exchanged with  $^{13}\text{CO}$  or  $\text{C}^{17}\text{O}$  ( $\sim 5$  mL at STP) in a heptane solvent at  $23^\circ\text{C}$  using 3 mg of Pd (10%) on  $\text{Al}_2\text{O}_3$  (Alfa Products, Danvers, MA). This catalyst causes essentially statistical (random) exchange in  $\sim 5$  min and can be readily removed by filtration. Crystals were then grown from  $\text{CH}_2\text{Cl}_2$ /pentane using a gradient technique. Crystallization times varied but were typically  $\sim 5$  days.

For protein NMR spectroscopy, we used both horse heart and sperm whale myoglobins (Sigma Chemical Company, St. Louis, MO). For  $^{13}\text{C}$  and  $^{17}\text{O}$  NMR, we typically purified myoglobin (Mb) by using a Sephadex G25 column and then grew needle or star-shaped crystal clusters from  $(\text{NH}_4)_2\text{SO}_4$  (83%, pH = 7.0). The crystals were then reduced on a Schlenk line using a few drops of  $(\text{NH}_4)_2\text{SO}_4$  solution containing  $\text{Na}_2\text{S}_2\text{O}_4$  (Sigma), and carbonylated with CO gas. Fourier transform infrared spectra were recorded on a Nicolet (Madison, WI) Magna-IR 750 spectrometer in order to deduce substate composition.

The  $A_0$  substate of MbCO was produced in  $\sim 95\%$  yield by converting Mb into the tetrazole derivative of His64<sup>30,31</sup> with CNBr (Aldrich Chemical Co., Milwaukee, WI) and  $\text{NaN}_3$  (Fisher Scientific, Fair Lawn, NJ). Crystals were grown from  $(\text{NH}_4)_2\text{SO}_4$  (78%, pH = 6.7) followed by reduction and carbonylation as described above.

The  $A_0$  substate of MbCO was produced in  $\sim 95\%$  yield by converting Mb into the tetrazole derivative of His64<sup>30,31</sup> with CNBr (Aldrich Chemical Co., Milwaukee, WI) and  $\text{NaN}_3$  (Fisher Scientific, Fair Lawn, NJ). Crystals were grown from  $(\text{NH}_4)_2\text{SO}_4$  (78%, pH = 6.7) followed by reduction and carbonylation as described above.

Sperm whale MbCO was used for  $^{57}\text{Fe}$  NMR and Mössbauer spectroscopy, and was from the same batch whose preparation has been described previously.<sup>32</sup>

**Spectroscopic Aspects.** Solid-state  $^{13}\text{C}$  and  $^{17}\text{O}$  NMR spectra were recorded using “home-built” spectrometers, which consist of 8.45 T 3.5 in. bore and 11.7 T 2.0 in. bore superconducting solenoid magnets (Oxford Instruments, Osney Mead, Oxford, U.K.), and Tecmag (Houston, TX) Aries and Libra data systems, together with a variety of other digital and rf circuitries. For rf pulse amplification, we used Amplifier Research (Souderton, PA) and Henry Radio (Los Angeles, CA) transmitters. Solid-state spectra were obtained by using 5 mm Doty Scientific (Columbia, SC) “magic-angle” sample-spinning (MAS) NMR probes, in some cases using sealed Wilmad (Buena, NJ) glass inserts. The  $90^\circ$  pulse widths varied but were typically  $\sim 4$   $\mu\text{s}$  for  $^{13}\text{C}$  and 5  $\mu\text{s}$  (solid  $90^\circ$  pulse) for  $^{17}\text{O}$ . For  $^{13}\text{C}$  NMR, we typically used  $^1\text{H}$ - $^{13}\text{C}$  cross polarization<sup>33</sup> with nonquaternary suppression.<sup>34</sup> Recycle times for  $^{13}\text{C}$  NMR were typically  $\sim 2$  s, while for  $^{17}\text{O}$  NMR, recycle times varied from 50 ms ( $A_1$  MbCO) to 1 s (Fe(TPP)(CO)(NMeIm)). Carbon-13 chemical shifts were referenced with respect to the low-field peak of adamantane, taken to be 38.5 ppm downfield from external tetramethylsilane, while  $^{17}\text{O}$  spectra were referenced with respect to an external sample of tap water. The convention that high-frequency, low-field, paramagnetic or deshielded shifts are more positive (International Union of Pure and Applied Chemistry, IUPAC,  $\delta$  scale) was used. Shift tensor elements use the convention that  $\delta_{11} \geq \delta_{22} > \delta_{33}$ .

The principal components of the chemical shift tensor,  $\delta_{11}$ ,  $\delta_{22}$ , and  $\delta_{33}$ , were deduced from the intensities of the individual spinning

(11) Johnson, K. A.; Olson, J. S.; Phillips, G. N., Jr. *J. Mol. Biol.* **1989**, *207*, 459–463. Eich, R. F.; Li, T.; Lemon, D. D.; Doherty, D. H.; Curry, S. R.; Aitken, J. F.; Mathews, A. J.; Johnson, K. A.; Smith, R. D.; Phillips, G. N. Jr.; Olson, J. S. *Biochemistry* **1996**, *35*, 6976–6983. Johnson, K. A.; Olson, J. S.; Smith, R. D.; Phillips, G. N., Jr. *Protein Data Bank in Crystallographic Databases – Information Content, Software Systems, Scientific Applications*; Data Commission of the International Union of Crystallography; file nos. 2MYA, 2MYB, 2MYC, and 2MYD, 2MYE, 1TES.

(12) Ray, G. B.; Li, X.-Y.; Ibers, J. A.; Sessler, J. L.; Spiro, T. G. *J. Am. Chem. Soc.* **1994**, *116*, 162–176. Ivanov, D.; Sage, J. T.; Keim, M.; Powell, J. R.; Asher, S. A.; Champion, P. M. *J. Am. Chem. Soc.* **1994**, *116*, 4139–4140.

(13) Lim, M.; Jackson, T. A.; Anfinrud, P. A. *Science* **1995**, *269*, 962–965.

(14) Park, K. D.; Guo, K.; Adebodun, F.; Chiu, M. L.; Sliagar, S. G.; Oldfield, E. *Biochemistry* **1991**, *30*, 2333–2347.

(15) Augspurger, J. D.; Dykstra, C. E.; Oldfield, E. *J. Am. Chem. Soc.* **1991**, *113*, 2447–2451.

(16) Oldfield, E.; Guo, K.; Augspurger, J. D.; Dykstra, C. E. *J. Am. Chem. Soc.* **1991**, *113*, 7537–7541.

(17) Yang, F.; Phillips, G. N., Jr. *J. Mol. Biol.* **1996**, *256*, 762–774.

(18) Norvell, J. C.; Nunes, A. C.; Schoenborn, B. P. *Science* **1975**, *190*, 568–570.

(19) Ascone, I.; Bianconi, A.; Dartyge, E.; Della Longa, S.; Fontaine, A.; Momentau, M. *Biochim. Biophys. Acta* **1987**, *915*, 168–171.

(20) Bianconi, A.; Congiu-Castellano, A.; Durham, P. J.; Hasnain, S. S.; Phillips, S. *Nature* **1985**, *318*, 685–687.

(21) Gerotheranassis, I.; Barrie, P. J.; Momentau, M.; Hawkes, G. E. *J. Am. Chem. Soc.* **1994**, *116*, 11944–11949.

(22) Trautwein, A.; Maeda, Y.; Harris, F. E.; Formanek, H. *Theor. Chim. Acta* **1974**, *36*, 67–76.

(23) Trautwein, A. In *Structure and Bonding*; Dunitz, J. D., Hemmerich, P., Holm, R. H., Ibers, J. A., Jørgensen, C. K., Neilands, J. B., Reinen, D., Williams, R. J. P., Eds.; Springer-Verlag: New York, 1974; Vol. 20, pp 101–166.

(24) Hirota, S.; Ogura, T.; Shinzawa-Itoh, K.; Yoshikawa, S.; Nagai, M.; Kitagawa, T. *J. Phys. Chem.* **1994**, *98*, 6652–6660. Hu, S.; Vogel, K. M.; Spiro, T. G. *J. Am. Chem. Soc.* **1994**, *116*, 11187–11188. Tsuboi, M. *Ind. J. Pure Appl. Phys.* **1988**, *26*, 188–191.

(25) Le, H.; Pearson, J. G.; deDios, A. C.; Oldfield, E. *J. Am. Chem. Soc.* **1995**, *117*, 3800–3807.

(26) Heller, J.; Laws, D. D.; Tomaselli, M.; King, D. S.; Wemmer, D. E.; Pines, A.; Havlin, R. H.; Oldfield, E. *J. Am. Chem. Soc.* **1997**, *119*, 7827–7831.

(27) Salzmann, R.; Ziegler, C.; Suslick, K. S.; Oldfield, E. Unpublished results.

(28) Peng, S.-M.; Ibers, J. A. *J. Am. Chem. Soc.* **1976**, *98*, 8032–8036.

(29) Webb, A. N.; Mitchell, J. J. *J. Phys. Chem.* **1959**, *63*, 1878–1885. Noack, K.; Ruch, M. *J. Organomet. Chem.* **1969**, *17*, 302–322.

(30) Adachi, S.-I.; Morishima, I. *Biochemistry* **1992**, *31*, 8613–8618.

(31) Kamiya, N.; Shiro, Y.; Iwata, T.; Iizuka, T.; Iwasaki, H. *J. Am. Chem. Soc.* **1991**, *113*, 1826–1829.

(32) Lee, H. C.; Gard, J. K.; Brown, T. L.; Oldfield, E. *J. Am. Chem. Soc.*, **1985**, *107*, 4087–4088. Chung, J.; Lee, H. C.; Oldfield, E. *J. Magn. Reson.* **1990**, *90*, 148–157.

(33) Pines, A.; Gibby, M. G.; Waugh, J. S. *J. Chem. Phys.* **1973**, *59*, 569–590.

(34) Opella, S. J.; Frey, M. H. *J. Am. Chem. Soc.* **1979**, *101*, 5854–5855.

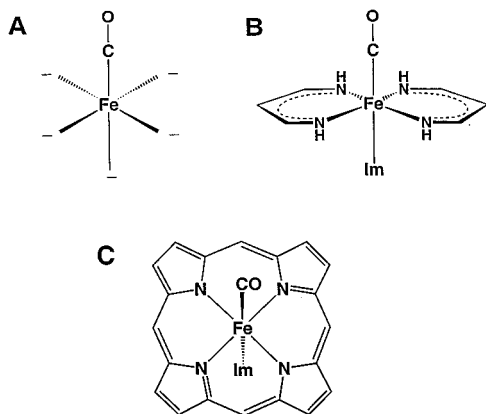


**Figure 1.** Fragments used for calculations. (A) Fe–C–O model used in electrostatic field calculations. Hyphens represent 0.4e point charges located at 2 Å from the Fe atom (the 5 closest nitrogen positions in a heme plus axial base). (B) Fe bis(amidinato)(CO)(N-methylimidazole) model system used for  $^{13}\text{C}$ ,  $^{17}\text{O}$  shielding calculations. (C) Full porphyrin model used for iron shift and efg calculations, Fe(porphine)(CO)(N-methylimidazole).

sidebands using several versions of the Herzfeld-Berger method,<sup>35</sup> as described below.

**Computational Aspects.** We carried out five series of density functional theory (DFT) calculations. In the first, we investigated how uniform and nonuniform electric fields influence the vibrational frequency and the  $^{17}\text{O}$  nuclear quadrupole coupling constant, as an extension of previous and more recent work on  $^{13}\text{C}$  NMR/ $^{17}\text{O}$  NMR/IR shift correlations.<sup>14–16,36</sup> These calculations used the small cluster shown in Figure 1A, which facilitated a full *E*-field vibrational/shift/electric field gradient (efg) analysis in a reasonable time period. The second set of calculations involved a study of how ligand tilt ( $\tau$ ) and bend ( $\beta$ ) alone affect the  $^{13}\text{C}$  and  $^{17}\text{O}$  shifts and shift anisotropies. This time a much larger model was used (Figure 1B), an Fe bis(amidinato)-(CO)(N-methylimidazole) system, which has been investigated previously by several groups.<sup>37,38</sup> Third, we investigated the  $^{57}\text{Fe}$  shifts and  $^{57}\text{Fe}$  Mössbauer quadrupolar splittings (equivalent to a determination of the electric field gradient tensor at the iron nucleus) using a full porphyrin, the Fe(porphinato)(CO)(N-methylimidazole) system shown in Figure 1C. Here, a large system was thought to be essential in order to adequately describe the  $^{57}\text{Fe}$ –ligand interactions. We also carried out a series of calculations on several chromium carbonyls and model hemes in which the orientation of the axial base was varied. Finally, we examined the shielding and the localized molecular orbital contributions to shielding at a single (linear) geometry.

The smallest model system is the one recently used to investigate charge field perturbation of  $^{13}\text{C}$ ,  $^{17}\text{O}$  shift– $\nu_{\text{CO}}$  (IR) correlations in proteins,<sup>36</sup> and consists of the octahedral arrangement of atoms and point charges shown in Figure 1A. The 0.4e point charges ensure a diamagnetic ground state and electroneutrality and are placed at 2 Å from the Fe atom. We used the deMon program<sup>39</sup> to evaluate the  $^{17}\text{O}$  efg and  $\nu_{\text{CO}}$ , employing Wachters' all electron basis set for iron (14s9p5d/8s5p5d)<sup>40,41</sup> together with an IGLO-III basis for C and O<sup>42</sup> and the Perdew–Wang (PW91) gradient-corrected exchange–correlation functional.<sup>43</sup> The  $^{17}\text{O}$  NQCC and  $\nu_{\text{CO}}$  values were evaluated in the presence of uniform electric fields applied along the Fe–C–O axis, having magnitudes from 0.02 to –0.02 au (1 au field = 5.14225  $\times$  10<sup>9</sup> V/cm), or in the presence of point charges of  $\pm e$  at 2 Å from the oxygen, along the Fe–C–O axis.

(35) Herzfeld, J.; Berger, A. *J. Chem. Phys.* **1980**, *73*, 6021–6030.

(36) deDios, A. C.; Earle, E. *J. Phys. Chem.* **1997**, *101*, 8132–8134.

(37) Strich, A.; Veillard, A. *Theor. Chim. Acta* **1981**, *60*, 379–383.

(38) Jewsbury, P.; Yamamoto, S.; Minato, T.; Saito, M.; Kitagawa, T. *J. Am. Chem. Soc.* **1994**, *116*, 11586–11587.

(39) deMon program: Salahub, D. R.; Fournier, R.; Mlynarski, P.; Papai, I.; St-Amant, A.; Ushio, J. In *Density Functional Methods in Chemistry*; Labanowski, J., Andzelm, J., Eds.; Springer: New York, 1991. St-Amant, A.; Salahub, D. R. *Chem. Phys. Lett.* **1990**, *169*, 387–392.

(40) Wachters, A. J. H. *J. Chem. Phys.* **1970**, *52*, 1033–1036. Wachters, A. J. H. *IBM Technol. Rep. RJ584* **1969**.

We next evaluated the  $^{13}\text{C}$  and  $^{17}\text{O}$  shieldings and shielding tensor elements, this time as a function of  $\tau$  and  $\beta$ . Here, the larger Fe bis(amidinato)(CO)(NMeIm) model shown in Figure 1B was used, since we were more interested in investigating the actual shifts, rather than the correlations between shifts and  $\nu_{\text{CO}}$ , and the elimination of the full vibrational analysis made computation of a shielding surface containing 35  $\tau, \beta$  values feasible. The nuclear shieldings were calculated with the sum-over-states density functional perturbation theory (SOS-DFPT) approach in its LOC1 approximation<sup>44</sup> using individual gauges for localized orbitals (IGLO)<sup>42</sup> as implemented in the deMon program.<sup>39</sup> We used the same iron basis as that shown above, while the C,O basis was reduced to IGLO-II.<sup>42</sup> Next, we investigated  $^{57}\text{Fe}$  NMR chemical shifts and the electric field gradients at  $^{17}\text{O}$ , and  $^{57}\text{Fe}$  (directly related to the  $^{57}\text{Fe}$  Mössbauer quadrupole splittings,  $\Delta E_Q$ ), again as a function of ligand tilt and bend. Since metal shifts have in the past been rather difficult to evaluate, we used a much larger fragment and increased the grid coarseness for our  $\tau, \beta$  study. We used a published porphyrin geometry<sup>28</sup> minus the C $^\beta$ -substituents, together with an axial imidazole oriented in the same way as reported in the crystal structure of carbonmonoxymyoglobin.<sup>45</sup> We carried out geometry optimizations of the Fe–C and C–O bond lengths at fixed ligand tilt and bend angles with the Gaussian 94/DFT program<sup>46</sup> using the B3LYP hybrid exchange–correlation functional,<sup>47</sup> Wachters' (62111111/3311111/3111) Fe basis set,<sup>40,41</sup> a 6-31G\* basis on the carbonyl group and the 5 nitrogen atoms, and a 3-21G basis on the remaining atoms. The nuclear shielding calculations were carried out in Gaussian 94/DFT using gauge-including atomic orbitals (GIAO),<sup>46</sup> a locally dense basis set scheme, and the B3LYP functional.<sup>47</sup> Wachters' basis set was used on the iron, 6-311++G(2d) on the CO group and five nitrogen atoms with 6-31G\* and 4-31G\*, on the second and third atom shells, respectively.

Heme model ligand shielding calculations were also done with G94/DFT using the BPW91 functional. For Fe(P)(CO)(pyr) (pyr = pyridine), the iron was represented with the LANLD2DZ effective core potential (ECP) with a (42111/2111/311) basis set,<sup>48</sup> or with the same ECP,<sup>49</sup> 6-311++G(2d) on the CO group, 6-31G\* on the nitrogen atoms, and 3-21G and STO-3G basis sets on the outermost atoms of the porphyrin ring. For Fe(TPP)(CO)(NMeIm), we used Wachters' iron basis set,<sup>40,41</sup> 6-311++G(2d) on the CO group and the five nitrogen atoms, 6-31G\* on the carbons bonded to the nitrogen atoms and 3-21G\* on the remaining atoms. For the Fe(C<sub>2</sub>Cap)(CO)(NMeIm), we used Wachters' Fe basis set, 6-311++G(2d) on the CO group and 6-31G\* on the rest of the atoms. This approach is basically that used by Bühl for  $^{57}\text{Fe}$  NMR chemical shift calculations in organometallic systems,

(41) Basis sets were obtained from the Extensible Computational Chemistry Environment Basis Set Database, Version 1.0, as developed and distributed by the Molecular Science Computing Facility, Environmental and Molecular Sciences Laboratory, which is part of the Pacific Northwest Laboratory, P.O. Box 999, Richland, WA 99352, and is funded by the U.S. Department of Energy under contract DE-AC06-76RLO 1830. Contact David Feller, Karen Schuchardt, or Don Jones for further information.

(42) Kutzelnigg, W.; Fleischer, U.; Schindler, M. In *NMR—Basic Principles and Progress*; Springer: Heidelberg, 1990; Vol. 28, p 1965.

(43) Perdew, J. P.; Wang, Y. *Phys. Rev. B* **1992**, *45*, 13244–13249.

(44) Malkin, V. G.; Malkina, O. L.; Casida, M. E.; Salahub, D. R. *J. Am. Chem. Soc.* **1994**, *116*, 5898–5908. Salahub, D. R. In *Theoretical and Computational Chemistry*; Politzer, P., Seminario, J. M., Eds.; Elsevier: New York, 1995.

(45) Abola, E. E.; Bernstein, F. C.; Bryant, S. H.; Koetzle, T. F.; Weng, J. *Protein Data Bank in Crystallographic Databases—Information Content, Software Systems, Scientific Applications*; Data Commission of the International Union of Crystallography; file no. 1MBC.

(46) Frisch, M. J.; Trucks, G. W.; Head-Gordon, M.; Gill, P. M. W.; Wong, M. W.; Foresman, J. B.; Johnson, B. G.; Schlegel, H. B.; Robb, M. A.; Replogle, E. S.; Gomperts, R.; Andres, J. L.; Raghavachari, K.; Binkley, J. S.; Gonzalez, C.; Martin, R. L.; Fox, D. J.; Defrees, D. J.; Baker, J.; Stewart, J. J. P.; Pople, J. A. *Gaussian94/DFT*; Gaussian, Inc.: Pittsburgh, PA, 1994.

(47) Becke, A. D. *J. Chem. Phys.* **1993**, *98*, 5648–5652. Lee, C.; Yang, W.; Parr, R. G. *Phys. Rev. B* **1988**, *37*, 785–789.

(48) Hay, P. J.; Wadt, W. R. *J. Chem. Phys.* **1985**, *82*, 270–283. Hay, P. J.; Wadt, W. R. *J. Chem. Phys.* **1985**, *82*, 284–298. Hay, P. J.; Wadt, W. R. *J. Chem. Phys.* **1985**, *82*, 299–310.

(49) Dolg, M.; Wedig, U.; Stoll, H.; Preuss, H. *J. Chem. Phys.* **1987**, *86*, 866–872.

**Table 1.**  $^{13}\text{C}$ ,  $^{17}\text{O}$  NMR Parameters for Fe Bis(amidinato)(CO)(NMeIm) as a Function of Ligand Tilt and Bend

ligand geometry		shielding tensor element			$\sigma_i$ (ppm)	$ \sigma_{22} - \sigma_{11} $ (ppm)	$ \sigma_{33} - \sigma_{11} $ (ppm)
tilt (deg)	bend (deg)	$\sigma_{11}$ (ppm)	$\sigma_{22}$ (ppm)	$\sigma_{33}$ (ppm)			
$^{13}\text{C}$							
0	0	-182.9	-169.9	263.1	-29.9	13	446
10	0	-182.8	-166.8	263.2	-28.8	16	446
20	0	-180.1	-161.1	263.9	-25.8	19	444
30	0	-172.9	-132.9	253.1	-17.6	40	426
40	0	-166.1	-63.1	214.9	-4.8	103	381
50	0	-156.9	47.1	115.1	1.8	204	272
0	10	-183.8	-169.8	264.2	-29.8	14	448
10	10	-179.9	-164.9	260.1	-28.2	15	440
20	10	-170.9	-160.9	257.1	-24.9	10	428
30	10	-160.1	-141.1	246.9	-18.1	19	407
40	10	-151.9	-77.9	212.1	-5.9	74	364
0	20	-183.9	-168.9	270.1	-27.6	15	454
10	20	-180.0	-162.0	260.0	-27.3	18	440
20	20	-170.8	-155.8	251.2	-25.1	15	422
30	20	-151.0	-148.0	239.0	-20.0	3	390
40	20	-139.0	-93.0	206.0	-8.7	46	345
0	30	-184.4	-167.4	282.2	-23.3	17	467
10	30	-178.9	-154.9	259.1	-24.9	24	438
20	30	-175.3	-146.3	244.7	-25.6	29	420
30	30	-161.6	-136.6	226.4	-23.9	25	388
40	30	-128.2	-109.2	191.8	-15.2	19	320
0	40	-184.6	-161.6	290.4	-18.6	23	475
10	40	-174.9	-137.9	244.1	-22.9	37	419
20	40	-179.0	-136.0	231.0	-28.0	43	410
30	40	-171.8	-127.8	199.2	-33.5	44	371
40	40	-125.7	-121.7	150.3	-32.4	4	276
0	50	-184.9	-154.9	296.1	-14.6	30	481
10	50	-174.9	-137.9	244.1	-22.9	37	419
20	50	-177.8	-128.8	201.2	-35.1	49	379
30	50	-171.1	-120.1	135.9	-51.8	51	307
40	50	-133.1	-118.1	6.9	-81.4	15	140
0	60	-177.0	-145.0	284.0	-12.7	32	461
10	60	-170.1	-131.1	217.9	-27.8	39	388
20	60	-160.0	-120.0	139.0	-47.0	40	299
30	60	-148.9	-121.9	7.1	-87.9	27	156
$^{17}\text{O}$							
0	0	-346.3	-323.3	410.7	-86.3	23	757
10	0	-345.1	-318.1	412.9	-83.4	27	758
20	0	-338.0	-282.0	402.0	-72.7	56	740
30	0	-335.1	-173.1	341.9	-55.4	162	677
40	0	-348.1	13.9	180.9	-51.1	362	529
50	0	-383.9	-114.9	206.1	-97.6	269	590
0	10	-357.9	-328.9	417.1	-89.9	29	775
10	10	-342.6	-313.6	410.4	-81.9	29	753
20	10	-327.9	-269.9	394.1	-67.9	58	722
30	10	-325.0	-167.0	329.0	-54.3	158	654
40	10	-336.8	4.2	155.2	-59.1	341	492
0	20	-381.7	-329.7	434.3	-92.4	52	816
10	20	-354.9	-314.9	417.1	-84.2	40	772
20	20	-319.8	-280.8	393.2	-69.1	39	713
30	20	-318.1	-179.1	318.9	-59.4	139	637
40	20	-330.2	-21.2	131.8	-73.2	309	462
0	30	-429.6	-324.2	465.6	-95.9	105	895
10	30	-380.3	-311.3	429.7	-87.3	69	810
20	30	-318.2	-303.2	394.8	-75.5	15	713
30	30	-310.9	-212.9	312.1	-70.6	98	623
40	30	-322.9	-60.9	112.1	-90.6	262	435
0	40	-489.0	-319.0	503.0	-101.7	170	992
10	40	-425.2	-305.2	444.8	-95.2	120	870
20	40	-354.9	-302.9	398.1	-86.6	52	753
30	40	-306.9	-267.9	312.1	-87.6	39	619
40	40	-314.1	-111.1	143.9	-93.8	203	458
0	50	-565.7	-309.7	545.3	-110.0	256	1111
10	50	-487.7	-299.7	457.3	-110.0	188	945
20	50	-423.7	-300.7	400.3	-108.0	123	824
30	50	-346.7	-301.7	333.3	-105.0	45	680
40	50	-300.7	-174.7	319.3	-52.0	126	620
0	60	-650.7	-297.7	570.3	-126.0	353	1221
10	60	-564.3	-295.3	457.7	-134.0	269	1022
20	60	-512.0	-301.0	381.0	-144.0	211	893
30	60	-454.0	-296.0	366.0	-128.0	158	820

**Table 2.**  $^{57}\text{Fe}$  NMR Shielding Parameters for  $\text{FeP}(\text{CO})(\text{NMeIm})$  as a Function of Ligand Tilt and Bend<sup>a</sup>

ligand geometry		shielding tensor elements			isotropic shielding $\sigma_i$	isotropic shift $\Delta_i$
tilt (deg)	bend (deg)	$\sigma_{11}$ (ppm)	$\sigma_{22}$ (ppm)	$\sigma_{33}$ (ppm)	(ppm)	(ppm)
0	0	-12266	-11180	-10961	-11469	8547
0	20	-12626	-12032	-11783	-12147	9225
0	40	-17295	-16797	-12126	-15405	12483
20	0	-12044	-11271	-10999	-11438	8516
20	20	-12330	-11921	-11542	-11931	9009
20	40	-14371	-13772	-12071	-13404	10482
40	0	-13900	-12937	-11236	-12691	9769
40	20	-14930	-13947	-11605	-13494	10572
40	40	-17521	-16316	-11982	-15273	12351

<sup>a</sup> Calculations were performed in Gaussian-94 using the B3LYP hybrid exchange correlation functional.

as described elsewhere.<sup>50</sup> The chromium carbonyl compounds were investigated with SOS-DFPT using the chromium DZVP (63321/5211/41+) basis set found in deMon,<sup>39</sup> IGLO-II basis sets on the remaining atoms, and the PW91 functional. The localized molecular orbital (LMO) contributions to the shielding in the  $\text{Fe}(\text{C}_2\text{Cap})(\text{CO})(\text{NMeIm})$  model were calculated with SOS-DFPT using the iron DZVP (63321/5211/41+) basis set found in deMon,<sup>39</sup> IGLO-II basis sets on the other atoms, and the PW91 functional.

Small molecule calculations were carried out on International Business Machines (Austin, TX) RS/6000 computers (models 340, 350, 360, 365 and 3CT), while the larger systems were investigated using Silicon Graphics/Cray Research (Mountain View, CA) Origin 200, Origin-2000, and Power Challenge multiple processor machines. The geometry optimizations and  $^{57}\text{Fe}$  shift and efg calculations were performed using the Silicon Graphics Power Challenge Array at the National Center for Supercomputing Applications, located in Urbana, IL, using up to 16 processors.

## Results and Discussion

The rapid improvements in computer speed over the past few years, together with the increasingly widespread applications of density functional theory, strongly suggest that it should now be possible to compute a wide range of spectroscopic observables in metalloproteins and related model systems.<sup>51</sup> The problem which exists, of course, is that the actual protein structures of interest are themselves the focus of debate. What is needed, therefore, are model compounds which have the same spectroscopic observables as do the proteins, but whose structures are more certain. Theoretical methods can then be used to predict the measured experimental parameters, validating the methods, after which aspects of protein structure can begin to be predicted using numerous observables measured on different proteins.

This is exactly the same approach which we have employed with amino acid residues in proteins in which quantum chemical methods were used to first reproduce chemical shifts (and shielding tensors) in amino acids<sup>52</sup> and proteins;<sup>53</sup> the process was then "inverted" and structural information derived from the experimental results in both peptides<sup>26</sup> and proteins.<sup>25</sup> In work with peptides, the rms (root-mean-square) deviations between X-ray experiment and NMR prediction were  $\sim 11^\circ$  for the

backbone torsion angles  $\phi$  and  $\psi$ . In this work, we use up to seven different observables, as follows, which should give improved structural predictions:

1.  $\delta_i$   $^{13}\text{C}$  = the isotropic carbon-13 NMR chemical shift;
2.  $\Delta\delta$   $^{13}\text{C}$  = the  $^{13}\text{C}$  NMR chemical shift anisotropy,  $|\delta_{33} - \delta_{11}|$ , also known as the tensor breadth or span;
3.  $\delta_i$   $^{17}\text{O}$  = the isotropic oxygen-17 NMR chemical shift;
4.  $e^2qQ/h$   $^{17}\text{O}$  = the oxygen-17 nuclear quadrupole coupling constant;
5.  $\delta_i$   $^{57}\text{Fe}$  = the isotropic iron-57 NMR chemical shift;
6.  $\Delta E_Q$   $^{57}\text{Fe}$  = the iron-57 Mössbauer quadrupolar splitting;
7.  $\nu_{\text{CO}}$  = the Fe-C-O infrared vibrational stretch frequency.

We consider first how the  $^{13}\text{C}$ ,  $^{17}\text{O}$ , and  $^{57}\text{Fe}$  NMR shift parameters vary with structure (tilt,  $\tau$ , and bend,  $\beta$ ), and we then investigate the accuracy of the experimental  $^{13}\text{C}$  tensor measurements, as well as how these tensors might be expected to vary as a function of axial base orientation and how individual localized molecular orbitals contribute to shielding. We then discuss experimental results on the  $A_0$  substate of MbCO, comparing them with experimental results obtained on a novel metalloporphyrin, Fe(5,10,15,20-tetraphenylporphyrin)(CO)(*N*-methylimidazole), which has a linear and untilted Fe-C-O structure.<sup>27</sup> We then use a Bayesian probability or *Z* surface method<sup>25,26</sup> to predict  $\tau$  and  $\beta$  in the  $A_0$  substate of MbCO, followed by a related analysis of  $\tau, \beta$  in the  $A_1$  substate, where electrostatic field effects also influence  $\nu_{\text{CO}}$  and the ligand NMR parameters. Finally, we compare the results of calculations of the electrostatic field perturbations with experiment and conclude with a general model for the three conformational substates,  $A_0$ ,  $A_1$ , and  $A_3$ , in terms of  $\tau, \beta$  and electrostatics, which is consistent with all of the experimental results, an approach which should be applicable to other ligands as well.

### Effects of Ligand Tilt and Bend on NMR Observables.

We first consider the effects of ligand tilt and bend on the following spectroscopic observables: the  $^{13}\text{C}$  isotropic shift, the  $^{13}\text{C}$  shift anisotropy, the  $^{17}\text{O}$  isotropic shift, and the  $^{57}\text{Fe}$  isotropic shift. Computed results for the model systems described above are given in Tables 1 and 2.

To begin with, we first compare these results with the experimental data published previously by ourselves and by others.<sup>14,21,54</sup> In these previous studies, the  $^{13}\text{C}$  and  $^{17}\text{O}$  NMR observables for CO in picket fence porphyrin were reported<sup>14,21</sup> in which CO is linear and untilted.<sup>55</sup> For  $^{13}\text{C}$ , at  $\tau = \beta = 0^\circ$  the calculated values (converted from the absolute shieldings using a value of 186 ppm for the absolute shielding of tetramethylsilane, ref 56) are  $\delta_{\text{iso}} = 215$  ppm,  $|\delta_{22} - \delta_{11}| = 13$  ppm, and  $|\delta_{33} - \delta_{11}| = 446$  ppm, to be compared with experimental values for the linear CO in picket fence porphyrin of  $\delta_{\text{iso}} = 205$  ppm,  $|\delta_{22} - \delta_{11}| = 8$  ppm, and  $|\delta_{33} - \delta_{11}| = 457$  ppm. For  $^{17}\text{O}$ , the calculated values (converted from the absolute shieldings using a value of 306 ppm for the absolute shielding of liquid water, ref 57) are  $\delta_{\text{iso}} = 392$  ppm,  $|\delta_{22} - \delta_{11}| = 23$  ppm, and  $|\delta_{33} - \delta_{11}| = 757$  ppm, to be compared with experimental values of  $\delta_{\text{iso}} = 372$  ppm,  $|\delta_{22} - \delta_{11}| < 30$  ppm, and  $|\delta_{33} - \delta_{11}| = 814$  ppm.<sup>14</sup> The errors seen on the isotropic shift are those which are typically found when a range of organometallic compounds

(50) Bühl, M. *Chem. Phys. Lett.* **1997**, 267, 251–257.

(51) Strohmlein, M.; Orendt, A. M.; Facelli, J. C.; Solum, M. S.; Pugmire, R. J.; Parry, R. W.; Grant, D. M. *J. Am. Chem. Soc.* **1997**, 119, 7114–7120. Yang, W.; Levy, M. *Symposium on Density Functional Theory, A Satellite Symposium of the 9th International Congress of Quantum Chemistry*; Durham, North Carolina, 1997.

(52) deDios, A. C.; Laws, D. D.; Oldfield, E. *J. Am. Chem. Soc.* **1994**, 116, 7784–7786.

(53) deDios, A. C.; Pearson, J. G.; Oldfield, E. *Science* **1993**, 260, 1491–1496.

(54) Gerothanassis, I. P.; Momentau, M.; Barrie, P. J.; Kalodimos, C. G.; Hawkes, G. E. *Inorg. Chem.* **1996**, 35, 2674–2679. Gerothanassis, I. P.; Momentau, M.; Hawkes, G. E.; Barrie, P. J. *J. Am. Chem. Soc.* **1993**, 115, 9796–9797.

(55) Hoard, J. L. In *Porphyrins and Metalloporphyrins*; Smith, K. M., Ed.; Elsevier: New York, 1975; pp 317–380.

(56) Jameson, K. J.; Jameson, C. J. *Chem. Phys. Lett.* **1987**, 134, 461–466.

(57) Wasylishen, R. E.; Mooibroek, S.; Macdonald, J. B. *J. Chem. Phys.* **1984**, 81, 1057–1059.

**Table 3.** Computed  $^{13}\text{C}$  and  $^{17}\text{O}$  NMR Shielding Results for Chromium Carbonyls and Model Hemes

system	$\sigma_{11}$ (ppm)	$\sigma_{22}$ (ppm)	$\sigma_{33}$ (ppm)	$\sigma_i$ (ppm)	$ \sigma_{11} - \sigma_{22} $ (ppm)
$^{13}\text{C}$					
Cr(CO) <sub>5</sub> (pyr), 0° <sup>a</sup>	-155.3	-154.2	258.5	-17.0	1.1
Cr(CO) <sub>5</sub> (pyr), 45° <sup>b</sup>	-155.4	-154.4	258.2	-17.2	1.0
Cr(CO) <sub>5</sub> (NMeIm), 0° <sup>c</sup>	-153.0	-151.5	257.3	-15.7	1.5
Cr(CO) <sub>5</sub> (NMeIm), 45° <sup>d</sup>	-153.4	-152.1	257.6	-15.9	1.3
Fe(TPP)(CO)(pyr) <sup>e</sup>	-188.9	-185.6	301.0	-24.5	3.3
Fe(TPP)(CO)(pyr) <sup>f</sup>	-188.6	-186.1	298.8	-25.3	2.5
Fe(TPP)(CO)(NMeIm) <sup>g</sup>	-173.6	-170.7	308.2	-12.0	2.9
Fe(TPP)(CO)(NMeIm) <sup>h</sup>	-199.2	-196.5	308.2	-29.2	2.7
Fe(C <sub>2</sub> Cap)(CO)(NMeIm) <sup>i</sup>	-196.6	-194.1	312.9	-25.9	2.5
Fe(C <sub>2</sub> Cap)(CO)(NMeIm), 0° <sup>j</sup>	-198.9	-195.0	315.9	-26.0	3.9
Fe(C <sub>2</sub> Cap)(CO)(NMeIm), 45° <sup>k</sup>	-198.3	-195.8	314.6	-26.5	2.5
$^{17}\text{O}$					
Cr(CO) <sub>5</sub> (pyr), 0° <sup>a</sup>	-286.2	-285.1	355.2	-72.0	1.1
Cr(CO) <sub>5</sub> (pyr), 45° <sup>b</sup>	-285.9	-283.2	355.5	-71.2	2.7
Cr(CO) <sub>5</sub> (NMeIm), 0° <sup>c</sup>	-270.8	-267.7	350.4	-62.7	3.1
Cr(CO) <sub>5</sub> (NMeIm), 45° <sup>d</sup>	-272.4	-269.0	369.6	-63.0	3.4
FeP(CO)(pyr) <sup>e</sup>	-284.5	-281.8	421.1	-48.4	2.7
FeP(CO)(pyr) <sup>f</sup>	-287.0	-283.5	419.1	-50.4	3.5
Fe(TPP)(CO)(NMeIm) <sup>g</sup>	-265.7	-264.6	449.2	-27.0	1.1
Fe(TPP)(CO)(NMeIm) <sup>h</sup>	-333.1	-331.6	446.5	-72.7	1.5
Fe(C <sub>2</sub> Cap)(CO)(NMeIm) <sup>i</sup>	-317.6	-316.2	447.5	-62.1	1.4
Fe(C <sub>2</sub> Cap)(CO)(NMeIm), 0° <sup>j</sup>	-320.5	-319.0	451.1	-62.8	1.5
Fe(C <sub>2</sub> Cap)(CO)(NMeIm), 45° <sup>k</sup>	-320.3	-318.4	449.0	-63.2	1.9

<sup>a</sup> Structure from ref 75, pyr plane along Cr–C<sub>eq</sub> axis, DZVP Cr/IGLO-II basis deMon calculation. <sup>b</sup> Structure from ref 75, pyr plane 45° to Cr–C<sub>eq</sub> axis, DZVP Cr/IGLO-II basis deMon calculation. <sup>c</sup> Structure from ref 75 with methylimidazole replacing pyridine, DZVP Cr/IGLO-II basis deMon calculation, NMeIm plane along Cr–C<sub>eq</sub> axis. <sup>d</sup> Structure from ref 75 with methylimidazole replacing pyridine, DZVP Cr/IGLO-II basis deMon calculation, NMeIm plane 45° to Cr–C<sub>eq</sub>. <sup>e</sup> Structure from ref 28 (minus the C<sup>β</sup>-substituents), Fe LANLD2DZ ECP/(42111/2111/311) basis set G94/DFT BPW91. See the text for details. <sup>f</sup> Structure from ref 28 (minus the C<sup>β</sup>-substituents), Fe ECP/(42111/2111/311) basis set G94/DFT BPW91. <sup>g</sup> Structure from ref 27 (with the C<sub>meso</sub> phenyl groups), riding model refinement, Wachters' Fe basis set, G94/DFT BPW91. <sup>h</sup> Structure from ref 27 (with the C<sub>meso</sub> phenyl groups), Fe–C/C–O geometry optimized, Wachters' Fe basis set, G94/DFT BPW91. <sup>i</sup> Structure from ref 60 (minus the ring substituents), Wachters' basis set, G94/DFT BPW91. <sup>j</sup> Same as *i* but with an axial base orientation of 0°. <sup>k</sup> Same as *i* but with an axial base orientation of 45°.

**Table 4.** Localized Molecular Orbital Contributions to CO Shielding in Fe(porphine)(CO)(N-methylimidazole)<sup>a</sup>

nucleus	LMO	$\sigma_{11}$	$\sigma_{22}$	$\sigma_{33}$	$\sigma_i$	$\Delta\sigma$
$^{13}\text{C}$	1s(C)	200.0	200.0	200.0	200.0	0
	LP(O)	-53.4	-53.3	3.3	-34.5	56.7
	3 × Bd(C≡O)	-88.6	-88.5	39.9	-45.7	128.5
	3 × Bd(Fe–C)	-233.5	-230.1	77.5	-128.7	311.0
	ΣAO(Fe)	2.6	2.3	-33.6	-9.5	-36.2
	Σ <sup>b</sup>	-172.9	-169.6	287.1	-18.4	460.0
	total <sup>c</sup>	-168.9	-166.1	308.4	-8.9	477.3
$^{17}\text{O}$	1s(O)	270.1	270.1	270.1	270.1	0
	LP(O)	-158.3	-157.8	34.7	-93.8	193.0
	3 × Bd(C≡O)	-259.5	-258.7	93.3	-141.7	352.8
	3 × Bd(Fe–C)	-157.5	-154.7	30.3	-93.9	187.8
	ΣAO(Fe)	0.4	0.3	-7.0	-2.1	-7.4
	Σ <sup>b</sup>	-304.8	-300.8	421.4	-61.4	726.2
	Total <sup>c</sup>	-299.0	-295.7	425.4	-56.4	724.4

<sup>a</sup> Values given are in ppm and were determined with the deMon program. <sup>b</sup> Sum of 5 LMO contributions shown. <sup>c</sup> Total LMO contributions.

are investigated, since the absolute isotropic shieldings are typically in error by at least 10–20 ppm,<sup>58,59</sup> and experimental errors on the individual tensor elements are also typically this large.<sup>60</sup> Thus, for these systems, there is generally good accord between theory and experiment. However, the known anticorrelation between  $^{13}\text{C}$  and  $^{17}\text{O}$  shifts seen in numerous proteins<sup>14</sup> is not apparent in the calculated results. In addition, the large

(~80 ppm) anisotropies,  $|\delta_{22} - \delta_{11}|$ , seen in hemoglobin, myoglobin, and some model systems<sup>21,54,61</sup> imply tilt angles between 30° and 40°. This translates to an 18 ppm difference in isotropic chemical shift, while the experimental difference between the protein and the picket fence porphyrin (linear) model is only 0.5 ppm. The results of Table 1 therefore indicate the following: (1) the calculations, structures, and/or theory have inadequacies, (2) some aspects of the shielding tensor measurements may be inaccurate, and/or (3)  $\tau, \beta$  effects are unimportant in controlling the overall changes in  $^{13}\text{C}, ^{17}\text{O}$  shifts seen in different proteins.

The results obtained for the  $^{57}\text{Fe}$  NMR chemical shifts are rather similar to those we found for the  $^{13}\text{C}, ^{17}\text{O}$  shift results given in Table 1 and are presented in Table 2. Experimentally, the isotropic chemical shift for  $^{57}\text{Fe}$  in MbCO has been reported by us and by others to be at ~8227 ppm downfield from Fe–(CO)<sub>5</sub>.<sup>32,62</sup> The DFT shielding calculations indicate an ~8547 ppm deshielding for  $\tau = \beta = 0^\circ$  (Table 2), but other  $\tau, \beta$  values are also consistent with experiment. However, highly bent structures such as  $\tau = 0, \beta = 40^\circ$  are some 4000 ppm too deshielded and are quite inconsistent with experiment. When taken together, the NMR results tend to support a linear geometry; therefore, we next investigate in more detail some of the NMR observations which tend to support nonlinearity.

**The Question of  $|\delta_{22} - \delta_{11}|$ .** One of the more puzzling results which emerges from the above calculations is that the large  $|\delta_{22} - \delta_{11}|$  values, which have been seen experimentally

(58) Kaupp, M.; Malkin, V. G.; Malkina, O. L.; Salahub, D. R. *Chem. Eur. J.* **1996**, *2*, 24–30.

(59) Salzmann, R.; Kaupp, M.; McMahon, M.; Oldfield, E. *J. Am. Chem. Soc.* **1998**, *120*, 4771–4783.

(60) Hawkes, G. E.; Sales, K. D.; Lian, L. Y.; Gobetto, R. *Proc. R. Soc. London A* **1989**, *424*, 93–111.

(61) Barrie, P. J.; Gerotheranassis, I. P.; Momentau, M.; Hawkes, G. E. *J. Magn. Reson. Ser. B* **1995**, *108*, 185–188. Barrie, P. J.; Gerotheranassis, I. P.; Momentau, M.; Hawkes, G. E. *J. Magn. Reson. Ser. B* **1995**, *108*, 185–188.

(62) LaMar, G. N.; Dellinger, C. M.; Sankar, S. S. *Biochem. Biophys. Res. Commun.* **1985**, *128*, 628–633. Baltzer, L.; Becker, E. D.; Tschudin, R. G.; Gansow, O. A. *J. Chem. Soc., Chem. Commun.* **1985**, 1040–1041.

**Table 5.** Experimental Determinations of Chemical Shift Tensor Elements in Mo(CO)<sub>6</sub> and Fe(TPP)(CO)(NMeIm)

system	method	$\mu$	$\rho$	$\delta_{11}$ (ppm)	$\delta_{22}$ (ppm)	$\delta_{33}$ (ppm)	$\delta_i$ (ppm)	$ \delta_{11} - \delta_{22} $ (ppm)
Mo(CO) <sub>6</sub>	static			338	338	-72	201	0
	least squares <sup>a</sup>	11.71	-0.91	346	328	-71	201	18
	Masfit <sup>b</sup>	11.93	-0.90	350	329	-76	201	21
	Z surface <sup>c</sup>	11.4	-1.0	336	336	-70	201	0
Fe(TPP)(CO)(NMeIm)								
	dry			390	315	-90	205	75
solvated				370	342	-98	205	28

<sup>a</sup> A least-squares fitting program kindly provided by R. E. Wasylshen. <sup>b</sup> A MAS NMR fitting program kindly provided by Alex Pines. <sup>c</sup> A Bayesian probability fitting program kindly provided by Dr. H. Le.

in several heme proteins and model compounds<sup>21,61</sup> and have in proteins been attributed to geometric ( $\tau, \beta$ ) distortions,<sup>21</sup> do not appear in the calculations. Or rather, when they do appear, they are accompanied by very large ( $\geq 15$  ppm) changes in isotropic shift from the linear, model compounds, effects which are not seen experimentally.

We therefore sought to see if such effects might be observable, computationally, in a series of model systems, by rotating the axial bases trans to CO, to see if, for example, metal  $d\pi \rightarrow$  ligand  $\pi^*$  "back-bonding" effects might in some cases cause anisotropies in the <sup>13</sup>C shielding tensor elements, a "proximal side" effect.<sup>38</sup> Results for Cr(CO)<sub>5</sub>(pyridine) and Cr(CO)<sub>5</sub>(*N*-methylimidazole) are presented in Table 3. Quite clearly, the anisotropies  $|\sigma_{22} - \sigma_{11}|$  due to two different orientations (0°, 45°) of two ligands (pyridine, *N*-methylimidazole) cause at most a 1.5 ppm asymmetry of the shielding tensor of the *trans*-CO, although the effect is somewhat larger for the *cis*-COs (data not shown) and for the <sup>17</sup>O shielding tensor elements as well, Table 3.

We next reasoned that the Cr(CO)<sub>5</sub>(B) model might simply be too crude a model to reproduce the effects seen in proteins, since it lacked the porphyrin macrocycle. We therefore investigated (a) a linear and untilted Fe-C-O system, FeP-(CO)(pyr), using two different Fe ECP/basis sets, resulting in a maximal  $|\sigma_{22} - \sigma_{11}|$  of 3.3 ppm, and (b) two Fe(TPP)(CO)-(NMeIm) structures, one with an exact X-ray structure deduced using a riding model refinement<sup>63</sup> for the terminal CO, the second containing a DFT/G94 optimized Fe-C-O geometry, Table 3. The Fe P (pyr) structure contained a relatively planar porphyrin,<sup>64</sup> while that in the *N*-methylimidazole model is clearly saddled—but no effects on  $|\sigma_{22} - \sigma_{11}|$  were seen. Finally, we investigated a structure based on Fe(C<sub>2</sub>Cap)(CO)-(NMeIm), an alternative close-to-planar porphyrin, using different axial base geometries, finding again only a 3.9 ppm maximal value for  $|\sigma_{22} - \sigma_{11}|$ , Table 3.

Interestingly, the anisotropies deduced using the Gaussian 94 program with the BPW91 functional tend to overestimate the  $\Delta\sigma$  values seen experimentally, an effect which we have also noted in metal-olefin calculations.<sup>65</sup> We therefore investigated the <sup>13</sup>C and <sup>17</sup>O shieldings again, this time with a full planar porphyrin and a linear and untilted Fe-C-O fragment, using SOS-DFPT with the PW91 functional. Here, we again wished to see to what extent addition of a symmetry-breaking axial *N*-methylimidazole might be responsible for  $\delta_{11} \neq \delta_{22}$ . Results, together with the localized molecular orbital contributions to shielding, are given in Tables 3 and 4. For <sup>13</sup>C,  $|\sigma_{22} - \sigma_{11}| = 3.6$  ppm and, for <sup>17</sup>O,  $|\sigma_{22} - \sigma_{11}| = 3.3$  ppm, essentially the same results obtained with the Gaussian-94 calculations.

(63) Schomaker, V.; Trueblood, K. N. *Acta Crystallogr. B* **1968**, *24*, 63–76.

(64) Kim, K.; Ibers, J. A. *J. Am. Chem. Soc.* **1991**, *113*, 6077–6081.

(65) Walter, T. H.; Thompson, A.; Keniry, M.; Shinoda, S.; Brown, T. L.; Gutowsky, H. S.; Oldfield, E. *J. Am. Chem. Soc.*, **1988**, *110*, 1065–1068.

However, the  $\Delta\sigma$  <sup>13</sup>C result of 477.3 ppm is clearly closer to experiment, confirming previous observations on metal-olefin complexes which indicated somewhat more accurate ligand shieldings using the SOS-DFPT/IGLO approach.

The results of Table 4 are also of interest since they give a very simple breakdown of the localized molecular orbital (LMO) contributions to <sup>13</sup>C, <sup>17</sup>O shielding. Apart from the 1s and lone pair contributions, both <sup>13</sup>C and <sup>17</sup>O shielding are dominated by C-O and Fe-C LMO contributions, with Fe-N<sub>im</sub> and Fe-N<sub>p</sub> contributions being quite minor. This, then, gives a logical explanation for the lack of major distal-base-orientation effects on the shieldings and emphasizes once again the unusual nature of observations of large  $|\sigma_{22} - \sigma_{11}|$  values which have been reported in some systems. Such effects seem not to be possible on the basis of tilt-bend, since they would be accompanied by very large changes in isotropic shifts, and are also not due to proximal side effects.

We then began to investigate to what extent  $|\sigma_{22} - \sigma_{11}|$  can actually be estimated using MAS NMR methods. As a first test, we reinvestigated the <sup>13</sup>C shielding tensors in Mo(CO)<sub>6</sub>. In previous work, we reported the spin-echo <sup>13</sup>C NMR spectrum of a static sample of Mo(<sup>13</sup>CO)<sub>6</sub>, where it is quite clear that the shielding tensor is, as expected, axially symmetric with  $\delta_{11} = \delta_{22} = 338$  ppm and  $\delta_{33} = -72$  ppm, Table 4. However, two different MAS/SSB fitting programs indicated an appreciable asymmetry,  $|\sigma_{22} - \sigma_{11}| = 18$  and 21 ppm, Table 5, using the MAS NMR sideband pattern reported previously.<sup>65</sup> In contrast, a Bayesian probability based Z surface method gives  $\delta_{11} = \delta_{22} = 336$  ppm and  $\delta_{33} = -72$  ppm, Table 5, in good agreement with the static line shape simulation. The most probable reason for this observation is, we believe, that *any* errors in the fitting procedure, due for example to limited signal-to-noise ratios, for an axially symmetric tensor will result in less than axial symmetry, in this case  $|\sigma_{22} - \sigma_{11}| \approx 20$  ppm. Apparently, the Bayesian probability approach gives more accurate results in such situations, as demonstrated from the results presented in Table 5.

A second possible source of experimental error might originate from the sample itself. For example, in a dry sample there could be heterogeneity, due to crystallographic defects. We therefore investigated two samples of Fe(TPP)(CO)-(NMeIm), Figure 2. In Figure 2A, we show the <sup>13</sup>C MAS NMR spectrum of a sample of Fe(TPP)(CO)(NMeIm) which had been dried in vacuo, while in Figure 2B we show a sample of crystals in excess mother liquor. The anisotropy seen in the dry sample is very large,  $|\sigma_{22} - \sigma_{11}| = 75$  ppm, similar to that reported in some protein and metalloporphyrin samples,<sup>21,61</sup> whereas in the solvated sample the anisotropy is considerably reduced to  $\sim 28$  ppm, Figure 2, a value which is within a 10–15 ppm estimated uncertainty per tensor element of axially symmetric. Interestingly, there is essentially no change in the isotropic shift, which is at  $\sim 205$  ppm in both cases, Table 4. The anisotropy of the two tensors,  $|\sigma_{33} - \sigma_{11}|$ , are very similar also, at 480 and 468 ppm.

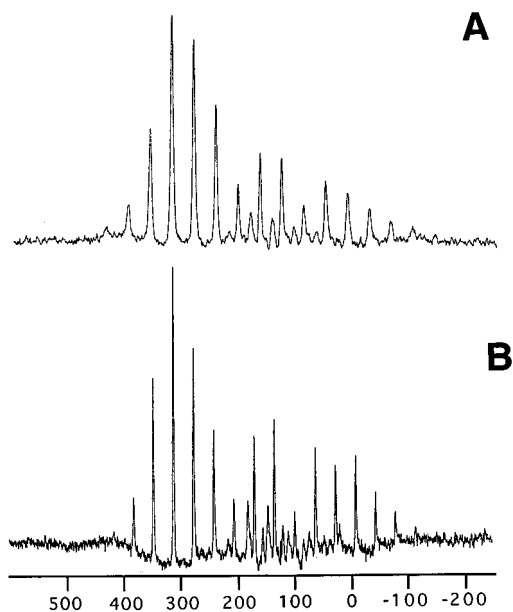


**Figure 2.** Experimental 90.5 MHz  $^{13}\text{C}$  CP-MAS NMR spectra of the  $A_0$  heme model, Fe(TPP)(CO)(NMeIm). (A) Dry powder sample spectrum,  $6 \mu\text{s}$   $90^\circ$  pulse widths, 5 ms mix time,  $\omega_r = 3.462$  kHz. (B) Solvated crystals, as in A but with  $\omega_r = 3.1$  kHz.

Therefore, it appears that while the isotropic shift and shift anisotropy can be quite reliably evaluated from MAS NMR spectra when using the Bayesian approach,  $|\delta_{22} - \delta_{11}|$  values are clearly more difficult to estimate reliably and perhaps will be less useful in structural analysis for this reason, especially when used alone.

**The  $A_0$  Substate.** We next move on to consider just what information can be deduced about metal–ligand geometries in proteins by using NMR, Mössbauer, and IR spectroscopic results. We first consider the case of the  $A_0$  substate of myoglobin, or heme proteins in general. Here, it is important to make a connection between the results obtained with relatively well-characterized model compounds, and with data obtained on proteins.

Fortunately, the spectroscopic parameters for Fe(TPP)(CO)(NMeIm) are very close to those found in the  $A_0$  substate of MbCO. The  $^{13}\text{C}$  NMR spectrum of an  $A_0$  substate (tetrazole) MbCO sample is shown in Figure 3, from which we find that  $\delta_i^{13}\text{C} = 205.8$  ppm and  $|\sigma_{33} - \sigma_{11}| = 435$  ppm, values which are within experimental error the same as those found for Fe(TPP)(CO)(NMeIm),  $\delta_i = 205$  ppm and  $|\delta_{33} - \delta_{11}| = 453$  ppm, Table 5. In addition, the  $^{17}\text{O}$ -isotropic shifts for  $A_0$  proteins and the TPP model are very similar:  $\delta_i^{17}\text{O} = 372$  ppm in the TPP model (exactly the same as found in solid  $\text{C}^{17}\text{O}$  picket fence porphyrin, ref 14) versus  $372 \pm 1$  ppm for a variety of  $A_0$  substate heme proteins.<sup>14</sup> The  $^{17}\text{O}$   $e^2qQ/h$  value in the TPP model from a nutation experiment, Figure 4, is 1.0 MHz, to be compared with 1.1 MHz on average for a range of  $A_0$  proteins from solution  $T_1$  measurements,<sup>14</sup> essentially the same as the 1.2 MHz we reported previously for  $\text{C}^{17}\text{O}$  picket fence porphyrin from a line shape simulation.<sup>14</sup> In addition, the  $\nu_{\text{CO}}$  in the TPP model,  $1969 \text{ cm}^{-1}$  (data not shown) is also that found for  $A_0$  substate proteins.<sup>14</sup> Finally, the  $^{57}\text{Fe}$  Mössbauer quadrupole splitting of  $0.35 \text{ mm sec}^{-1}$  in the TPP model<sup>66</sup> is close to that found in  $A_0$  substate mutant proteins (P. G. Debrunner, private communication). Taken together, these results tend to suggest that the linear Fe–C–O bonded Fe(TPP)(CO)(NMeIm) system

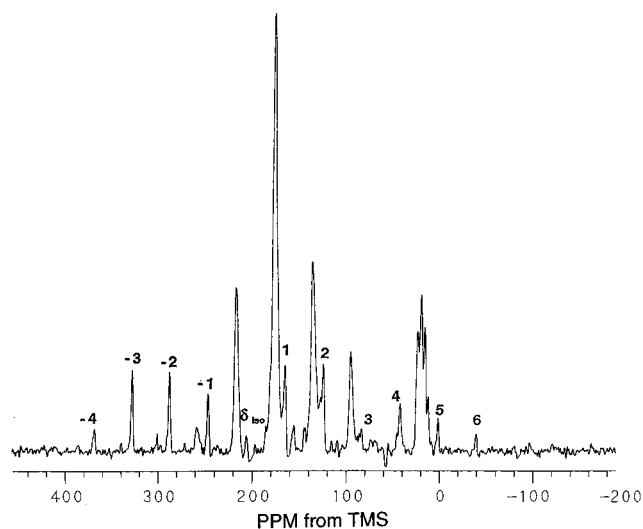


**Figure 3.** Proton-decoupled (90.46 MHz, 8.45 T)  $^{13}\text{C}$  MAS NMR spectrum of HisE7 tetrazoyl  $^{13}\text{CO}$ -myoglobin crystals obtained with  $^1\text{H}$  cross polarization and nonquaternary suppression at a spinning speed of 3.4 kHz. Experimental conditions were  $-25^\circ\text{C}$ , 71 146 scans, 2 s recycle time,  $3.9 \mu\text{s}$  ( $90^\circ$ ) pulse width, 3 ms mix time,  $60 \mu\text{s}$  dephasing period (NQS), and 100 Hz line broadening due to exponential multiplication.

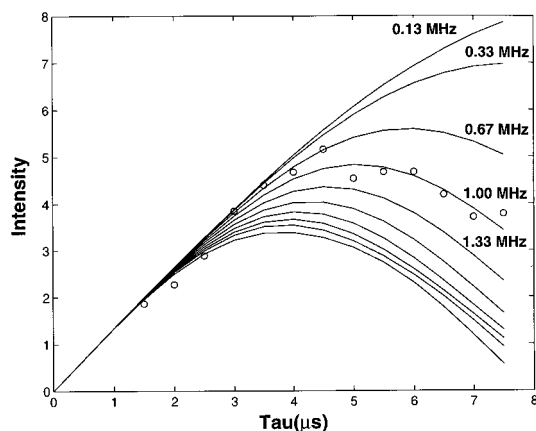


**Figure 4.**  $^{17}\text{O}$  NMR nutation plot for Fe(TPP)(CO)(NMeIm). The solution  $90^\circ$  pulse width (on  $\text{H}_2\text{O}$ ) was  $10.5 \mu\text{s}$ . The nutation simulation yields  $e^2qQ/h = 1.0 \pm 0.2$  MHz, with an assumed asymmetry parameter  $\eta = 0$ .

and CO picket fence porphyrin, are good model systems for the  $A_0$  substates of heme proteins, since the  $^{13}\text{C}$   $\delta_i$ ,  $^{13}\text{C}$   $|\sigma_{33} - \sigma_{11}|$ ,  $^{17}\text{O}$   $\delta_i$ ,  $^{17}\text{O}$   $e^2qQ/h$ ,  $\nu_{\text{CO}}$ , and  $^{57}\text{Fe}$   $\Delta E_Q$  results are very similar. However, the possibility exists that there are other, alternative solutions for  $\tau, \beta$ , which can also explain all of the spectroscopic observables, which we next investigate by using the Bayesian or Z surface approach.<sup>25,26</sup>

The basic idea here is that if a parameter surface is computed as a function of tilt and bend,  $P(\tau, \beta)$ , then the likelihood that a given experimental value of a parameter,  $P^{\text{expt}}$ , is given by a particular set of  $\tau, \beta$  values is given by<sup>25,26</sup>

$$1/Z = e^{-(P^{\text{expt}} - P^{\text{calcd}}_{\tau, \beta})^2/W} \quad (1)$$

where  $W$  is a search width parameter.<sup>25,26</sup> If the computed value of the parameter,  $P^{\text{calcd}}_{\tau, \beta}$  is identical to that found experimentally,  $P^{\text{expt}} - P^{\text{calcd}}_{\tau, \beta} = 0$ , then  $Z = 1$ , a high probability solution. On the other hand, if  $P^{\text{expt}} - P^{\text{calcd}}_{\tau, \beta} \neq 0$ , then  $Z \rightarrow 0$ , a low probability solution. The method can be readily extended from a one-parameter or  $1/Z$  solution to multiple parameters, so long

(66) Havlin, R. H.; Godbout, N.; Salzmann, R.; Wojdelski, M.; Arnold, W.; Schulz, C. E.; Oldfield, E., *J. Am. Chem. Soc.* **1998**, *120*, 3144–3151.

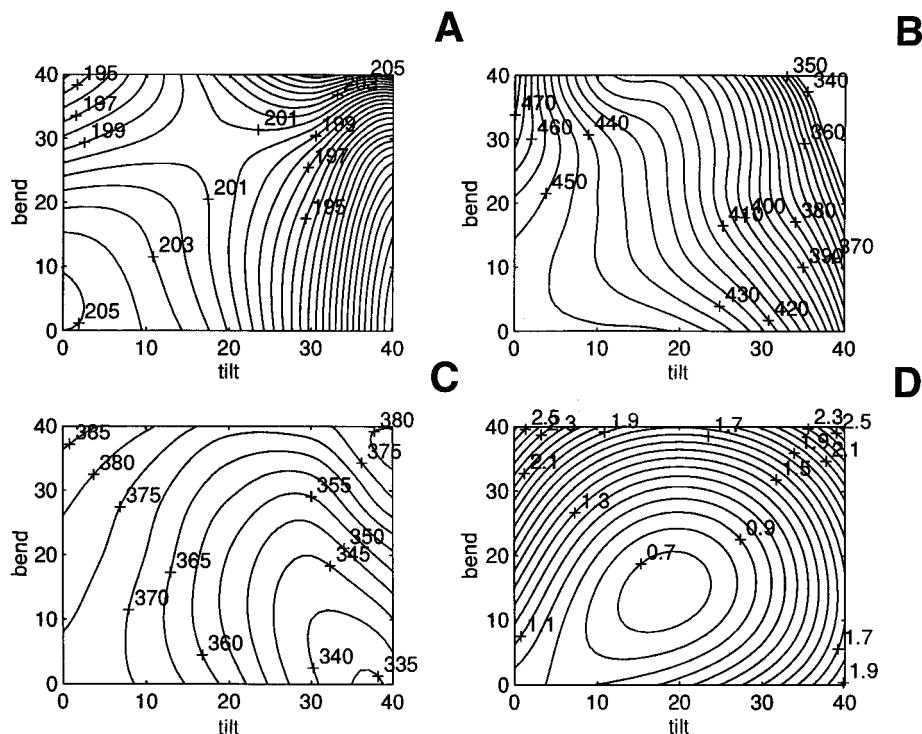


**Figure 5.** NMR parameter surfaces as a function of tilt and bend, computed using the deMon program with the Fe bis(amidinato)(CO)(*N*-methylimidazole) model system. (A)  $^{13}\text{C}$ -isotropic shielding surface, scaled to  $\delta_i = 205$  ppm at  $\tau = \beta = 0$ , the experimental shift value for Fe-(TPP)(CO)(NMeIm) and picket fence porphyrin. (B)  $^{17}\text{O}$ -isotropic shielding surface, scaled to  $\delta_i = 372$  ppm at  $\tau = \beta = 0$ . (C)  $^{13}\text{C}$   $\Delta\sigma$  ( $|\sigma_{33} - \sigma_{11}|$ ) shielding anisotropy surface (ppm). (D)  $^{17}\text{O}$  NQCC surface (in MHz).

as the form of  $P(\tau, \beta)$  is known. In this case, we investigate the use of four parameters: the  $^{13}\text{C}$  NMR isotropic chemical shift, the  $^{13}\text{C}$  NMR chemical shift anisotropy, the  $^{17}\text{O}$  NMR isotropic chemical shift, and the  $^{17}\text{O}$  nuclear quadrupole coupling. The four  $Z$  surfaces are then combined as follows:

$${}^4Z(\tau, \beta) = {}^1Z(^{13}\text{C}, \delta_i) {}^1Z(^{13}\text{C}, |\delta_{33} - \delta_{11}|) {}^1Z(^{17}\text{O}, \delta_i) {}^1Z(^{17}\text{O}, e^2qQ/h) \quad (2)$$

The actual computed parameter ( $P$ ) surfaces are shown in Figure 5 and the individual  ${}^1Z$  surfaces are shown in Figure 6. Here, it is important to note that the isotropic chemical shift surfaces have been converted from the chemical shifts computed theoretically using corrections of 10.3 ppm ( $^{13}\text{C}$ ) and 22.3 ppm ( $^{17}\text{O}$ ), such that the two known linear and untilted Fe(porphyrin)-(CO)(NMeIm) models have the experimental isotropic chemical shift. For the  $|\delta_{33} - \delta_{11}|$  and  $^{17}\text{O}$  NQCC, this conversion was not necessary. In some  $Z$  surfaces, there are high probability solutions over wide regions of  $\tau, \beta$  space, Figure 6. However, when all four parameters are simultaneously included, only the  $\tau = \beta \leq 2^\circ$  region has a high probability, as shown in Figure 6. From this we conclude that the  $A_0$  substate of MbCO, and other heme proteins, has a linear Fe-C-O geometry. This is certainly not an unreasonable conclusion since all of the spectroscopic observables are virtually identical between  $A_0$  MbCO and the new Fe(TPP)(CO)(NMeIm) model system. That is, a linear and untilted Fe-CO is one possible solution. However, the results of Figures 5 and 6, when considered together, are very important since they give no evidence for alternate  $\tau, \beta$  conformational solutions which might also fit the experimental  $^{13}\text{C}$  and  $^{17}\text{O}$  NMR results.

**The  $A_1$  Substate.** We next consider the  $A_1$  substate of MbCO and other heme proteins, such as hemoglobin. Here, there are additional parameter surfaces to be considered. In

particular, there are several published results on the  $^{57}\text{Fe}$  Mössbauer quadrupole splitting,  $\Delta E_Q$ ,<sup>67</sup> as well as additional reports on the  $^{57}\text{Fe}$  NMR isotropic chemical shift.<sup>32,62</sup> We show in Figure 7 the  $^{13}\text{C}$  and  $^{17}\text{O}$  MAS NMR spectra of the  $A_1$  substate of MbCO, from which we deduce  $\delta_i$ , and for  $^{13}\text{C}$ ,  $|\delta_{33} - \delta_{11}|$  and these and other parameter results are collected in Table 6.

There are clearly isotropic chemical shift differences, in addition to  $^{17}\text{O}$  quadrupole coupling constant differences, between the  $A_0$  and  $A_1$  protein and model system results. These differences could, in principle, have two origins: either they are structural or they are electrostatic. In previous work, we and others have suggested an electrostatic origin for the observed frequency shifts and NQCC changes in the ligand atoms. The principal reason for this was that extremely good correlations are found between the various experimental parameters:  $\delta_i(^{17}\text{O})$ ,  $\delta_i(^{13}\text{C})$ ,  $e^2qQ/h(^{17}\text{O})$ , and  $\nu_{\text{CO}}$  (14) (as shown for example in Figure 8). Here, we plot three correlations based on protein NMR/IR results, and in addition, we show the location of the new model compound, Fe(TPP)(CO)(NMeIm),  $\Delta$ , as well as recent  $\delta_i^{13}\text{C}/\nu_{\text{CO}}$  results for a  $\text{C}_2\text{Cap}$  porphyrin, which has highly perturbed frequency shifts.<sup>68</sup> Essentially all of the protein and model compound results lie on the same curves, implying a similar mechanism is responsible for these correlations. Indeed, with the inclusion of the  $\text{C}_2\text{Cap}$  results and results for the peroxidases, the correlation covers a range of almost  $100 \text{ cm}^{-1}$  in  $\nu_{\text{CO}}$ , Figure 8.

In earlier work, we reproduced to a modest extent the slopes of these correlations by using an electrostatic field to polarize a CO molecule: a model for MbCO. More recently, this model has been improved to include the electroneutral FeCO species

(67) Debrunner, P. G. In *Iron Porphyrins*; Lever, A. B. P., Gray, H. B., Eds.; VCH Publishers: New York, 1989; Vol. 3, pp 139–234.

(68) Jones, R. D.; Budge, J. R.; Ellis, P. E., Jr.; Linard, J. E.; Summerville, D. A.; Basolo, F. J. *Organomet. Chem.* **1979**, *181*, 151–158.

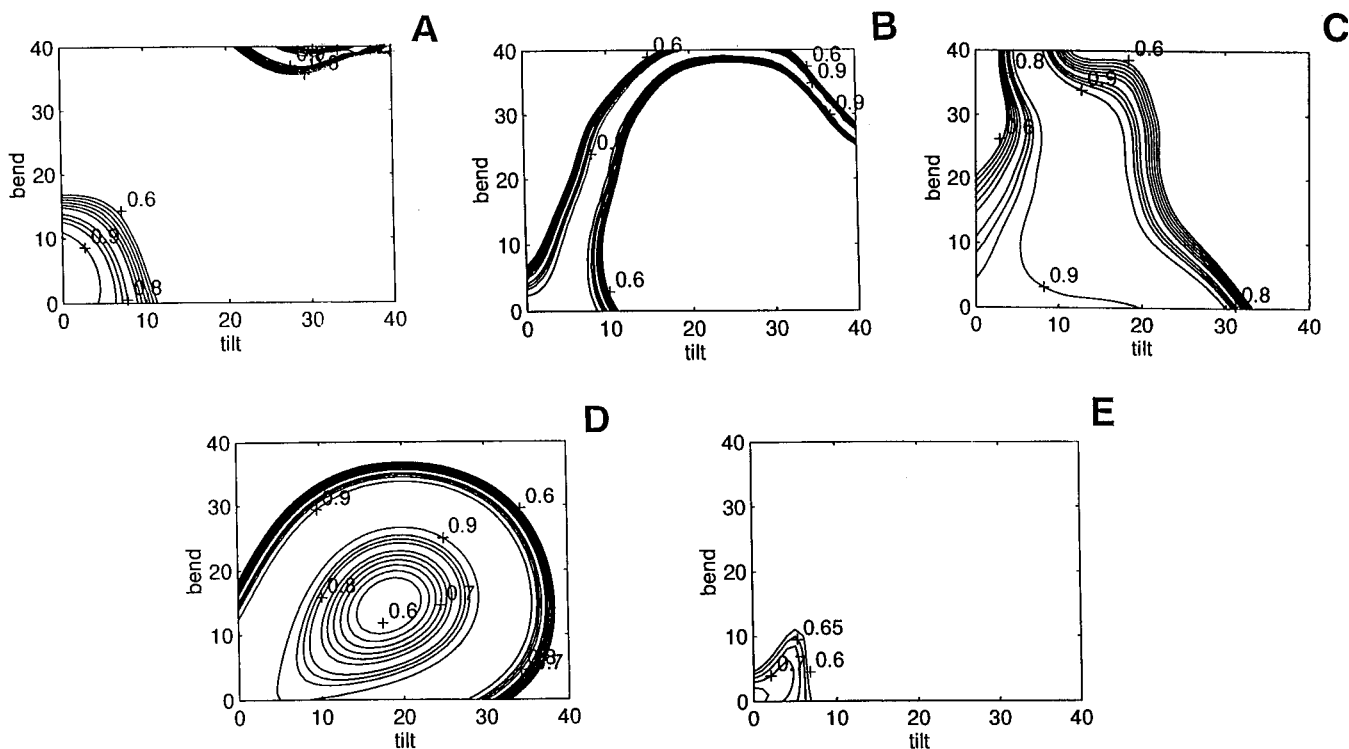


**Figure 6.** Z surfaces as a function of tilt and bend for the  $A_0$  substate of MbCO. (A)  $^{13}\text{C}$ -isotropic shift  $^1Z$  surface. (B)  $^{17}\text{O}$ -isotropic shift  $^1Z$  surface. (C)  $^{13}\text{C}$  CSA  $^1Z$  surface. (D)  $^{17}\text{O}$  NQCC  $^1Z$  surface. (E)  $^{13}\text{C}_{\text{iso}}$ ,  $^{13}\text{C}_{\text{CSA}}$ ,  $^{17}\text{O}_{\text{iso}}$ ,  $^{17}\text{O}_{\text{NQCC}}$   $^4Z$  surface. The values given are the likelihoods  $n\sqrt{^nZ}$ .

shown in Figure 1A, and excellent accord was found for the  $^{17}\text{O}$  isotropic shift versus  $\nu_{\text{CO}}$  correlation and a more modest correlation for the  $^{13}\text{C}$  isotropic shift versus  $\nu_{\text{CO}}$  correlation.<sup>14,36</sup> We have now computed the  $^{17}\text{O}$   $e^2qQ/h$  versus  $\nu_{\text{CO}}$  correlation, using both uniform field and point charges to perturb the FeCO fragment.<sup>69</sup> We find derivatives  $\partial(e^2qQ/h)/\partial(\nu_{\text{CO}})$  of 11 kHz/ $\text{cm}^{-1}$  for the uniform field model and 16 kHz/ $\text{cm}^{-1}$  for the point charge model, to be compared with 11.28 kHz/ $\text{cm}^{-1}$  determined experimentally.<sup>14,36,69</sup> The averages of the uniform field and point charge IR/NMR correlation lines are shown in Figure 8 and strongly support the idea that  $E$ -fields determine the major changes seen between all the  $A_i$  substates, since the correlations between  $^{13}\text{C}_i$ ,  $^{17}\text{O}_i$ ,  $^{17}\text{O}$   $e^2qQ/h$ , and  $\nu_{\text{CO}}$  are well reproduced by the calculations, although the absolute values of the properties are not exactly the same as the protein or porphyrin results because of the simplicity of the FeCO fragment.

Our results also suggest that  $E$ -field effects for the  $A_0$  substate are close to zero, since there is no change in  $\nu_{\text{CO}}$  in Fe(TPP)-(CO)(NMeIm) in solution and in the crystalline solid state and there is no distal fragment available to polarize the CO and generate an  $E$ -field effect.

If these ideas are correct, it should therefore be possible to extend the Bayesian probability approach to investigate the most likely conformation of the  $A_1$  substate, simply by using the known  $\nu_{\text{CO}}$  to make a small correction to the observed  $^{13}\text{C}/^{17}\text{O}$  shifts and the  $^{17}\text{O}$   $e^2qQ/h$  values, using the theoretical correlation lines shown in Figure 8. In addition, for the  $A_1$  substates of heme proteins, there is an extensive database of  $^{57}\text{Fe}$  NMR chemical shifts and  $^{57}\text{Fe}$  Mössbauer quadrupole splittings,  $\Delta E_Q$ , which can also in principle be used to investigate  $\tau, \beta$  effects.

We show therefore in Figure 9 computed  $^{57}\text{Fe}$  NMR isotropic chemical shift and  $^{57}\text{Fe}$  Mössbauer quadrupole splitting surfaces as a function of  $\tau, \beta$  for a model Fe(P)(CO)(NMeIm) metallo-

cycle. The  $^{57}\text{Fe}$  NMR chemical shieldings, Figure 9A, computed using the G94/DFT GIAO method described above are given in Table 3 and have been converted into  $^{57}\text{Fe}$  NMR chemical shifts,  $\delta_i$ , in ppm from Fe(CO)<sub>5</sub> using the following equation

$$^{57}\text{Fe } \delta(\text{shift, ppm from Fe(CO)}_5) = -2922 - \sigma(\text{calcd, ppm}) \quad (3)$$

where  $\sigma(\text{calcd, ppm})$  is the isotropic shielding given in Table 2. The value of  $-2922$  ppm has been established by using the databases of Bühl (50) augmented with three model calculations on metallocycles Fe(TPP)(Me<sub>2</sub>S)(NMeIm), Fe(TPP)(<sup>i</sup>PrNC)-(NMeIm) and Fe(TPP)(CO)(NMeIm), using the experimental shifts of cytochrome *c*,<sup>70</sup> alkyl isocyanide myoglobins and carbonmonoxymyoglobin, as will be described in detail elsewhere.<sup>71</sup>

The Mössbauer quadrupole splittings are derived from the electric-field gradient tensor, computed in Gaussian-94 using the B3LYP hybrid exchange correlation functional. In Mössbauer spectroscopy, the observed spectra of low spin  $d^6$  iron complexes generally consist of a quadrupole split doublet having a peak separation,  $\Delta E_Q$ , which is related to the elements of the electric field gradient tensor at the nucleus by

$$\Delta E_Q = \frac{1}{2}eQV_{zz}\left(1 + \frac{\eta^2}{3}\right)^{1/2} \quad (4)$$

where  $e$  is the electron charge,  $Q$  the quadrupole moment of the  $I^* = 3/2$ , 14.4 keV excited state,  $V_{zz}$  is the largest component of the efg tensor, and by convention

(70) Baltzer, L. *J. Am. Chem. Soc.* **1987**, *109*, 3479–3481.

(71) Godbout, N.; Havlin, R.; Salzman, R.; Debrunner, P. G. *Oldfield, E. J. Phys. Chem. A* **1998**, *102*, 2342–2350.

(69) deDios, A. C.; Earle, E. Unpublished results.

**Table 6.** Experimental Parameters for Fe(TPP)(CO)(NMeIm), A<sub>0</sub> and A<sub>1</sub> Myoglobins

system	<sup>13</sup> C <sub>i</sub> (ppm)	<sup>13</sup> C <sub>CSA</sub> (ppm)	<sup>17</sup> O <sub>i</sub> (ppm)	<sup>17</sup> O <sub>NQCC</sub> (MHz)	<sup>57</sup> Fe <sub>i</sub> (ppm)	ΔE <sub>Q</sub> (mm/s)	IR (cm <sup>-1</sup> )
Fe(TPP)(CO)(NMeIm)	205.0 <sup>a</sup>	453 <sup>a</sup>	372 <sup>a</sup>	1.0 <sup>a</sup>		0.35 <sup>b</sup>	1969 <sup>c</sup>
A <sub>0</sub> myoglobin	205.5 <sup>d</sup>	435 <sup>a</sup>	372 <sup>d</sup>	1.1 <sup>d</sup>			1969 <sup>d</sup>
A <sub>1</sub> myoglobin	207.2 <sup>d</sup>	447 <sup>a</sup>	366 <sup>a</sup>	0.8 <sup>d</sup>	8227 <sup>e</sup>	0.37 <sup>f</sup>	1944

<sup>a</sup> Determined in this work. <sup>b</sup> Reference 66. <sup>c</sup> Determined in Nujol. <sup>d</sup> Reference 14. <sup>e</sup> Reference 32. <sup>f</sup> Reference 22.

$$\eta = \frac{V_{xx} - V_{yy}}{V_{zz}} \quad (5)$$

$$|V_{zz}| > |V_{yy}| > |V_{xx}| \quad (6)$$

In the presence of an applied field, each molecule has its efg oriented differently in the field, and a powder spectrum is observed. However, methods are available to evaluate such powder averages as a function of  $V_{ii}$ , from which  $\Delta E_Q$  and the sign of  $\Delta E_Q$  can be deduced.<sup>72,73</sup> Unfortunately, there has been some debate as to the value of  $Q$ , the quadrupole moment of the excited iron nucleus. Here, we use a recent and reportedly very precise value,  $Q = 0.16 \times 10^{-28} \text{ cm}^2$ , to convert the computed  $V_{ii}$  values (in atomic units) to the Mössbauer quadrupole splittings,  $\Delta E_Q$  (mm/s) using eq 4.

Elsewhere, we have investigated the <sup>57</sup>Fe Mössbauer quadrupole splittings in 14 organometallic model systems<sup>66</sup> and find a <0.2 mm/s rms error between theory and experiment, which gives an idea as to the accuracy with which  $\Delta E_Q$  can be determined. Figure 9B shows the Mössbauer  $\Delta E_Q(\tau, \beta)$  surface computed for our model metalloporphyrin. In separate work, we have found experimentally<sup>66</sup> that the quadrupole splitting of the model system Fe(5,10,15,20-tetraphenylporphyrin)(CO)-(N-methylimidazole) is 0.35 mm/s, essentially the same as that seen in MbCO, where values of 0.363–0.373 have been reported.<sup>23,67</sup> Large basis set efg calculations on the complete TPP system yield a  $\Delta E_Q$  of 0.44 mm/s, to be compared with our smaller model, having  $\Delta E_Q = 0.52 \text{ mm/s}$ .<sup>66</sup> Since we know that the linear Fe–C–O TPP model has a 0.35 mm/s  $\Delta E_Q$ , we have used a –0.17 mm/s correction to the  $\tau, \beta$   $\Delta E_Q$  surface. This is necessary, since otherwise we would conclude the TPP model is slightly bent, which it is not—although we should note that even an unscaled (0.52 mm/s  $\tau = \beta = 0^\circ$ ) surface only changes the final  $\tau, \beta$  predictions by about 1°.

For the iron-57 NMR chemical shift, the <sup>1</sup>Z surface, Figure 9C, shows a most likely solution close to  $\tau = \beta = 0^\circ$ , although given the 800 ppm rms error seen for three metalloprotein models<sup>71</sup> (as reflected in our 787 ppm value for  $W$ ), clearly considerable distortions are allowed, based solely on the <sup>57</sup>Fe NMR chemical shift. The same can be said for the iron-57 Mössbauer  $\Delta E_Q$  <sup>1</sup>Z surface, Figure 9D. For example a  $\tau = \beta = 20^\circ$  solution is spectroscopically permissible, albeit not so energetically. These results simply reinforce the idea that multiple  $Z$  surfaces need to be combined in order to obtain a  $\tau, \beta$  solution which is consistent with *all* of the observables. We therefore show in Figure 10 the <sup>6</sup>Z surface obtained by considering all of the NMR and Mössbauer data:

$${}^6Z(\tau, \beta) = {}^1Z({}^{13}\text{C}, \delta_i) {}^1Z({}^{13}\text{C}, \text{CSA}) {}^1Z({}^{17}\text{O}, \delta_i) \times {}^1Z({}^{17}\text{O}, e^2qQ/h) {}^1Z({}^{57}\text{Fe}, \delta_i) {}^1Z({}^{57}\text{Fe}, \Delta E_Q) \quad (7)$$

The most likely solution occurs for  $\tau = 4^\circ, \beta = 7^\circ$ , essentially a linear and untilted Fe–C–O fragment. This result gives good predictions for the isotropic <sup>13</sup>C NMR chemical shift, the <sup>13</sup>C

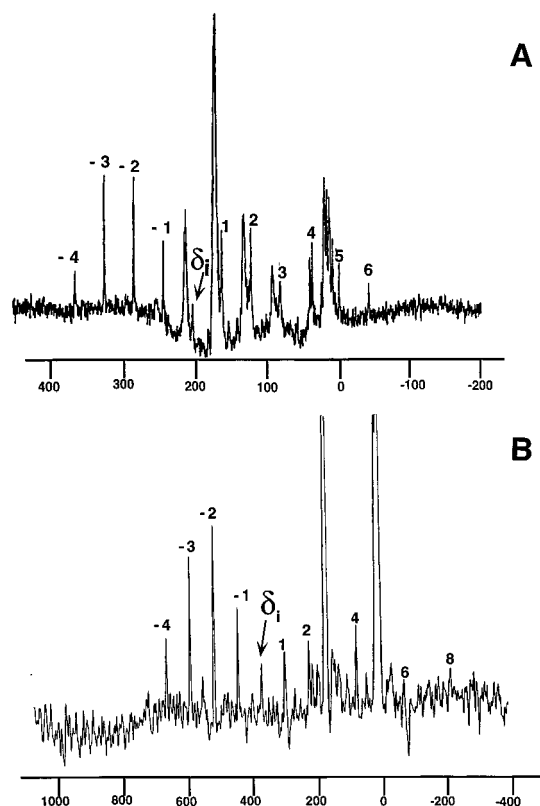


**Figure 7.** Experimental <sup>13</sup>C and <sup>17</sup>O solid-state MAS NMR spectra of A<sub>1</sub> CO horse myoglobin crystals at pH 7. (A) <sup>13</sup>C CP-NQS NMR spectrum at 90.5 MHz, –25 °C, 7 μs 90° pulse widths, 60 μs dephasing, a 3 ms mix time, ω<sub>r</sub> = 3.7 kHz, recycle = 2 s, 88 944 scans, convolution difference processing. (B) 67.8 MHz (11.7 T) <sup>17</sup>O NMR spectrum of C<sup>17</sup>O-myoglobin crystals. Experimental conditions were –24 °C, 1 048 000 scans, 50 ms recycle time, a 5.0 μs (solid 90°) pulse width, and 25 Hz line broadening due to exponential multiplication. The spinning sidebands are numbered.

NMR chemical shift anisotropy, the isotropic <sup>17</sup>O NMR chemical shift, the <sup>17</sup>O nuclear quadrupole coupling constant, the <sup>57</sup>Fe NMR chemical shift, and the <sup>57</sup>Fe Mössbauer quadrupole splitting, as summarized in Table 7. Moreover, the result shown in Figure 10 is not dominated by a single, narrow solution for a particular spectroscopic parameter. For situations in which there are extensive amounts of data, for example <sup>13</sup>C NMR shifts of amino acid residues in proteins, the  $W$  value chosen in eq 1 can be related to the rms or standard deviation of the data set.<sup>25,26</sup> However, when only single-point experiments are available,  $W$  values have to be deduced by estimating errors on a calculation (and experiment) in the absence of a large body of data. In such situations, a single badly chosen  $W$  value may dominate the final  $Z$  surface. We have tested for this possibility by selectively removing individual  $Z$  surfaces from the result shown in Figure 10, to generate the six individual <sup>5</sup>Z surfaces shown in Figure 11. In all cases, the <sup>5</sup>Z results are very similar to the <sup>6</sup>Z results, with  $\tau, \beta$  values very similar to the <sup>4</sup>Z result obtained with the A<sub>0</sub> substate, Figure 6. That is, in no case does a single  $Z$  surface dominate the final result. The actual  $W$ -values used, together with a theoretical-versus-experimental comparison of

(72) Zimmerman, R. *Nucl. Inst. Methods* **1975**, 128, 537–541.

(73) Münck, E.; Groves, J. L.; Tumolillo, T. A.; Debrunner, P. G. *Computer Phys. Commun.* **1973**, 5, 225–238.

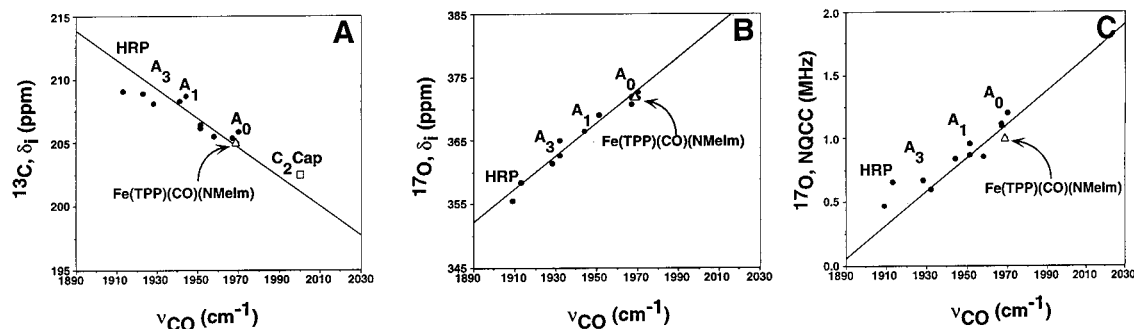


**Figure 8.** Experimental (solid circles, from ref 14) and theoretical (solid lines, from refs 36 and 69) NMR/IR correlation plots for heme proteins and model compounds. (A)  $^{13}\text{C}$ -isotropic shift versus  $\nu(\text{C}-\text{O})$ . (B)  $^{17}\text{O}$ -isotropic shift versus  $\nu(\text{C}-\text{O})$ . (C)  $^{17}\text{O}$  NQCC versus  $\nu(\text{C}-\text{O})$ . The solid circles represent results obtained on proteins. The open triangles are the results obtained on the TPP model described in the text, and the open square is C<sub>2</sub>-cap. The solid lines are the theoretical correlation lines, based on Fe-C-O model systems<sup>36,69</sup> offset along the ordinate to intersect the data at  $\nu_{\text{CO}} = 1969 \text{ cm}^{-1}$ , to facilitate comparison.

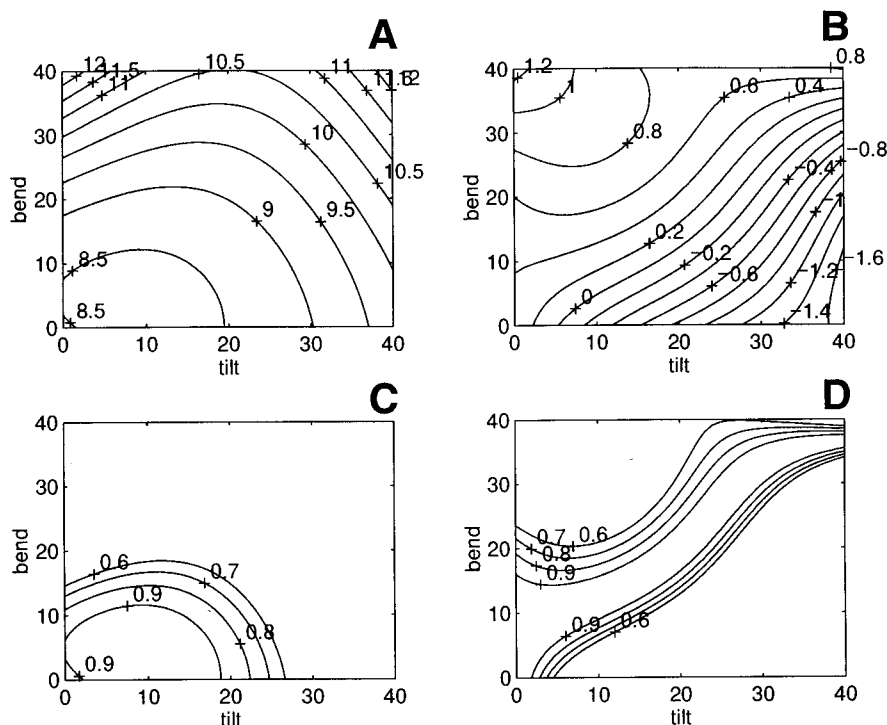


**Figure 9.**  $^{57}\text{Fe}$  NMR isotropic chemical shift and Mössbauer quadrupole splitting tilt-bend surfaces and associated Z surfaces for the A<sub>1</sub> substate. (A)  $^{57}\text{Fe}$ -isotropic shift parameter surface. (B)  $^{57}\text{Fe}$  quadrupole splitting parameter surface, offset by  $-0.17 \text{ mm/s}$  to reproduce the Fe(TPP)(CO)-(NMelm) model system. (C)  $^{57}\text{Fe}$ -isotropic shift  $^{1/2}Z$  surface. (D)  $^{57}\text{Fe}$  quadrupole splitting  $^{1/2}Z$  surface. The values shown in A are the  $^{57}\text{Fe}$  shifts, in  $10^3 \text{ ppm}$ , and in B are the  $\Delta E_Q$  in  $\text{mm/s}$ . The values in C and D are the  $^{1/2}Z$  likelihoods.

all of the results obtained, are given in Table 7. Note that both  $\tau, \beta$  and  $E$ -field contributions are included. On average, the mean  $^{13}\text{C}, ^{17}\text{O} =$  isotropic shift error is 0.4 ppm, the  $^{13}\text{C}$  CSA error is 7 ppm, the efg error is 0.13 MHz, the  $^{57}\text{Fe}$   $\Delta E_Q$  error is 0.05 mm/s, and the  $^{57}\text{Fe}$ -isotropic shift error is 179 ppm. For the  $^{13}\text{C}$  and  $^{17}\text{O}$  shifts, as noted previously, the isotropic shifts were scaled to fit the linear TPP and picket fence models, as was the  $^{57}\text{Fe}$  Mössbauer surface. This is necessary in part to account for basis and functional deficiencies and is similar to the scaling we have used previously with amino acid shielding in peptides<sup>26</sup> and proteins.<sup>25</sup> For the  $^{13}\text{C}$  CSA, the  $^{17}\text{O}$  NQCC, and the  $^{57}\text{Fe}$  shifts, no scaling was used since the CSAs and efgs were in good accord with the model compound experiments, and for  $^{57}\text{Fe}$ , the solid-state  $^{57}\text{Fe}$  shift is unknown. Indeed, the use of solely unscaled and uncorrected parameter surfaces yields  $\tau = \beta = 6^\circ$ , in good agreement with the more rigorous computations described above.

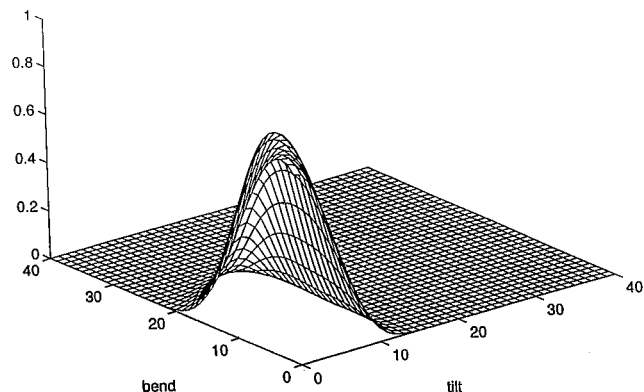


**Figure 10.**  $^6Z$  surface for A<sub>1</sub> protein conformational substate using  $^{13}\text{C} \delta_i$ ,  $^{17}\text{O} \delta_i$ ,  $^{57}\text{Fe} \delta_i$ ,  $^{13}\text{C} \Delta\delta$ ,  $^{17}\text{O}$  NQCC, and  $^{57}\text{Fe} \Delta E_Q$  surfaces. The maximum is at  $\tau = 4^\circ$ ,  $\beta = 7^\circ$ . The maximum Z value is  $^6\sqrt{^6Z} = 0.92$ .

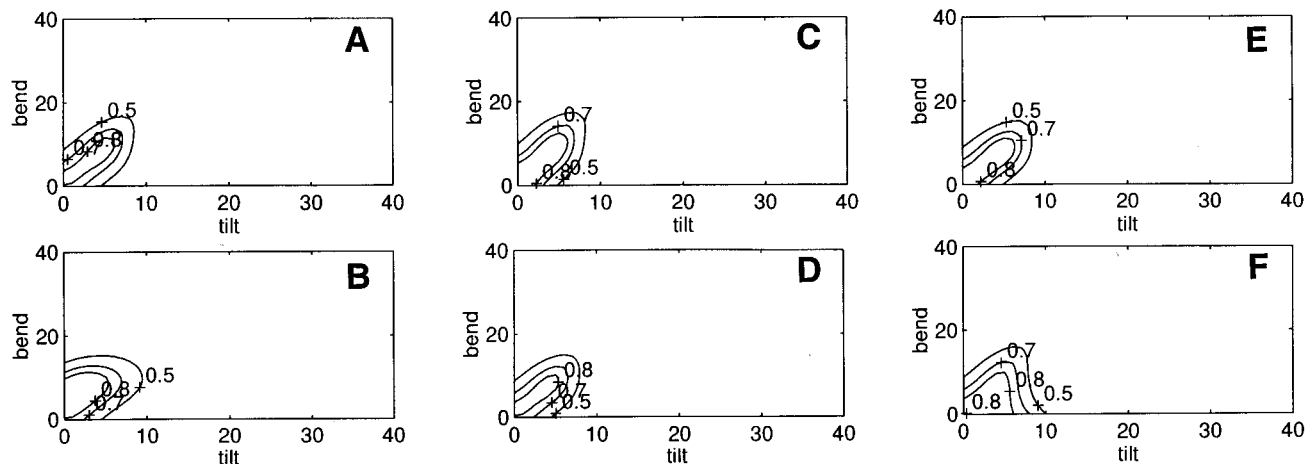


**Figure 11.** Six  ${}^5Z$  surfaces of  $A_1$  myoglobin illustrating the effect of removing each Z surface. **A**,  ${}^{13}\text{C}$  isotropic shift removed. **B**,  ${}^{17}\text{O}$  isotropic shift removed. **C**,  ${}^{57}\text{Fe}$  isotropic shift removed. **D**,  ${}^{13}\text{C}$  CSA removed. **E**,  ${}^{17}\text{O}$  NQCC removed. **F**,  ${}^{57}\text{Fe}$  quadrupolar splitting removed. The contours represent  ${}^5\sqrt{{}^5Z}$  and decrease in 0.1 intervals.

**Table 7.** Calculated and Experimental Spectroscopic Parameters for Typical  $A_0$  and  $A_1$  CO–Heme Protein Substates

parameter	$A_0$			$A_1$		
	calcd	exptl	$W$	calcd	exptl <sup>a</sup>	$W$
${}^{13}\text{C}_{\text{iso}}$ (ppm)	205	205.3	3.2	206.8	207.2	3.2
${}^{13}\text{C}_{\text{CSA}}$ (ppm)	446	435	28.0	445	447	28.0
${}^{17}\text{O}_{\text{iso}}$ (ppm)	372	372.4	4.5	366.7	366	4.5
${}^{17}\text{O}_{\text{NQCC}}$ (MHz)	0.9	1.1	0.6	0.64	0.8	0.6
${}^{57}\text{Fe}_{\Delta E_Q}$ (mm/s)				0.30	0.37	0.4
${}^{57}\text{Fe}_{\text{iso}}$ (ppm)				8406	8227	787

<sup>a</sup> The electrical contributions to  ${}^{13}\text{C}$   $\delta_i$ ,  ${}^{17}\text{O}$   $\delta_i$  and the  ${}^{17}\text{O}$  NQCC were obtained from the theoretical correlation lines shown in Figure 8.

In summary then, the use of density functional theory now permits the relatively accurate prediction of  ${}^{13}\text{C}$  NMR chemical shifts and shift tensor elements,  ${}^{17}\text{O}$  NMR shifts,  ${}^{17}\text{O}$  nuclear quadrupole coupling constants,  ${}^{57}\text{Fe}$  NMR chemical shifts and  ${}^{57}\text{Fe}$  Mössbauer quadrupole splittings in metalloporphyrin model systems and in metalloproteins themselves. Experimental results on linear and untilted Fe–C–O metalloporphyrins are essentially the same as those found in the  $A_0$  substate of heme proteins. This implies that the proteins could also contain linear and untilted Fe–C–O units, and the results of additional DFT calculations rule out alternative, distorted conformations for the  $A_0$  substate. With the  $A_1$  substates of heme proteins, there are small changes in the ligand NMR and electric field gradient parameters, but these can now be rather well described, especially for the  $\delta_i$   ${}^{17}\text{O}$  and  ${}^{17}\text{O}$  NQCC/ $\nu_{\text{CO}}$  correlations, in terms of purely electrostatic field effects, calculable via quantum chemistry. For the  $A_1$  substate, we also have available the  ${}^{57}\text{Fe}$  NMR isotropic shifts and the  ${}^{57}\text{Fe}$  Mössbauer quadrupole splittings,  $\Delta E_Q$ . These are not expected to change appreciably with  $E$ -field effects, since these in general come from the distal histidine and as such are expected to affect primarily the  ${}^{17}\text{O}$  shift and  ${}^{17}\text{O}$  NQCC. The  ${}^{57}\text{Fe}$  shift and  ${}^{57}\text{Fe}$  efg can therefore be used as additional parameters with which to test ideas about metal–ligand geometry. Using the simple porphyrin model, we find errors of about 200 ppm for the  ${}^{57}\text{Fe}$  shift (8227 ppm expt, 8406 ppm calcd), a small number when compared with the  $\sim 1000$ – $3000$  ppm errors found for  $20^\circ$ ,  $40^\circ$  bent geometries. The same can be said for the  ${}^{57}\text{Fe}$  Mössbauer results, where highly bent geometries result in very large errors in computed  ${}^{57}\text{Fe}$  efgs, while linear and untilted geometries give computed Mössbauer quadrupole splittings,  $\Delta E_Q$ , which are very close to those found experimentally.

We believe these results therefore indicate that the  $A_0$  and  $A_1$  substates of MbCO and, by inference other heme proteins, contain linear Fe–C–O geometries, since all six spectroscopic observables: the carbon-13, oxygen-17, and iron-57 NMR isotropic chemical shifts, the  ${}^{13}\text{C}$  shift anisotropy, the  ${}^{17}\text{O}$  quadrupole coupling constant, and the  ${}^{57}\text{Fe}$  Mössbauer quadrupole splitting, are all close to those found via DFT. This improves upon the more limited results using just DFT energies alone or solely IR data, which appear to leave some uncertainties as to the actual  $\tau, \beta$  values present in proteins, with in some cases large distortions reported as possible (see, e.g., ref 74). The changes in the ligand NMR/IR shifts from system to system seen previously can be readily accounted for in terms of  $E$ -field effects, again using DFT methods. These results also suggest that the  $A_3$  substate is very close to linear and untilted, as are the unusually shifted peroxidase “post- $A_3$ ” substates, since (i) all points fall on the universal  $\delta_i$   ${}^{17}\text{O}/\delta_i$   ${}^{13}\text{C}/{}^{17}\text{O}$  NQCC/ $\nu_{\text{CO}}$  correlations, (ii) the slopes of these correlations can now be computed via use of DFT methods, and (iii) these correlations are not due to  $\tau, \beta$ .

While an argument might be made that the highly distorted Fe–C–O structures are only found in  $P2_1$  sperm whale MbCO, the Mössbauer surface results give no support to this idea, and indeed DFT calculations at the X-ray geometries overestimate  $\Delta E_Q$  by 500%,<sup>66</sup> while assumption of a linear geometry gives results within the 0.1–0.2 mm/s rms error expected. Indeed, the fact that both solution and solid-state data can all be combined together using the Bayesian probability approach to give unique solutions, which permit an explanation of seven different observables from three different spectroscopies, NMR, IR, and Mössbauer, which also cover a dozen or more proteins and model systems ( $\text{C}_2\text{Cap}$ ,  $A_0$ ,  $A_1$ ,  $A_3$ , peroxidases), gives some confidence in the use of such methods for investigating related structural questions in other systems as well.

## Conclusions

The results we have shown above are of interest for three reasons. First, they represent the first comprehensive investigation of  ${}^{13}\text{C}$  NMR chemical shifts,  ${}^{13}\text{C}$  NMR chemical shift

(74) Spiro, T. G.; Kozlowski, P. M. *J. Biol. Inorg. Chem.* **1997**, *2*, 516–520. Slebochnick, C.; Ibers, J. A. *J. Biol. Inorg. Chem.* **1997**, *2*, 521–525. Vangberg, T.; Bocian, D. F.; Ghosh, A. *J. Biol. Inorg. Chem.* **1997**, *2*, 526–530. Sage, T. J. *J. Biol. Inorg. Chem.* **1997**, *2*, 537–543.

(75) Ries, W.; Bernal, I.; Quast, M.; Albright, T. A. *Inorg. Chim. Acta* **1984**, *83*, 5–15.

anisotropies,  $^{17}\text{O}$  NMR chemical shifts,  $^{17}\text{O}$  nuclear quadrupole couplings,  $^{57}\text{Fe}$  NMR chemical shifts, and  $^{57}\text{Fe}$  Mössbauer quadrupole splittings in metalloproteins and model systems using modern density functional methods and experiment. Second, our results indicate that all of the spectroscopic observables can be well accounted for in terms of linear, untilted Fe–C–O bonding, with weak electrostatic fields controlling the differences seen between  $A_0$  and  $A_1$  substates. Third, we have extended the use of the Z surface method, based on Bayesian probability, to explore the topic of ligand tilt and bend: the results give no support for distorted geometries, either in solution or in the solid-state. Combining the results of NMR, IR, and Mössbauer spectroscopic measurements in this way should be a general approach for predicting metal–ligand geometries in other systems as well, for example with  $\text{O}_2$  and RNC metal–ligand bonding in heme proteins, where the more conventional IR/Raman-based methods alone are less sensitive.

**Acknowledgment.** This work was supported by the United States Public Health Service (National Heart, Lung and Blood

Institute grant HL-19481). This work was also supported in part by use of the SGI/Cray Origin 2000 and Power Challenge clusters at the National Center for Supercomputing Applications (funded in part by the US National Science Foundation grant CHE-970020N). We also gratefully acknowledge Professor Dennis Salahub, Drs. Vladimir Malkin and Olga Malkina for providing a copy of their deMon and SOS-DFPT deMon program, and Professor U. Nienhaus for initial FT-IR measurements. M.T.M. is a National Institutes of Health Molecular Biophysics Training Grant Trainee, A.C.D. is an American Heart Association, Inc., Illinois Affiliate, Postdoctoral Fellow (1994–1995). R.S. is a Swiss National Science Foundation Postdoctoral Fellow (1996–1997) and an American Heart Association, Inc., Illinois Affiliate, Postdoctoral Fellow (1997–1998). D.D.L. is a Colgate-Palmolive Fellow. R.H.H. is a Barry Goldwater Fellow.

JA973272J